

Accurate Landmarking of Three-Dimensional Facial Data in the Presence of Facial Expressions and Occlusions Using a Three-Dimensional Statistical Facial Feature Model

Xi Zhao, *Student Member, IEEE*, Emmanuel Dellandréa, Liming Chen, *Member, IEEE*, and Ioannis A. Kakadiaris, *Senior Member, IEEE*

Abstract—Three-dimensional face landmarking aims at automatically localizing facial landmarks and has a wide range of applications (e.g., face recognition, face tracking, and facial expression analysis). Existing methods assume neutral facial expressions and unoccluded faces. In this paper, we propose a general learning-based framework for reliable landmark localization on 3-D facial data under challenging conditions (i.e., facial expressions and occlusions). Our approach relies on a statistical model, called 3-D statistical facial feature model, which learns both the global variations in configurational relationships between landmarks and the local variations of texture and geometry around each landmark. Based on this model, we further propose an occlusion classifier and a fitting algorithm. Results from experiments on three publicly available 3-D face databases (FRGC, BU-3-DFE, and Bosphorus) demonstrate the effectiveness of our approach, in terms of landmarking accuracy and robustness, in the presence of expressions and occlusions.

Index Terms—Facial expression, fitting, landmarks, occlusion, statistical face model, 3-D face feature.

I. INTRODUCTION

THE RECENT emergence of 3-D facial data has provided an alternative to overcome the challenges in 2-D face recognition, caused by pose changes and lighting variations [6]. Although 2.5D/3-D face data acquisition is known to be insensitive to changes in lighting conditions, the data need to be pose normalized and correctly registered for further face analysis (e.g., 3-D face matching [20], tracking [33], recogni-

tion [26], [28], and facial expression analysis [34]). As most of the existing registration techniques assume the availability of some 2.5D/3-D face landmarks, a reliable localization of these facial feature points is essential.

A. Related Work

Although there is no general consensus yet, we consider stable facial landmarks to be the fiducial points defined by anthropometry [9] that have consistent reproducibility even in adverse conditions such as facial expression or occlusion. Stable facial landmarks generally include the nose tip, the inner eye corners, the outer eye corners, and the mouth corners. Such landmarks are not only characterized by their own properties, in terms of local texture and local shape, but are also characterized by their global structure resulting from the morphology of the face. Therefore, local feature information and the configurational relationships of landmarks are jointly important for accurate and robust face landmarking. This finding is coherent with human studies on face analysis suggesting that both local features and configurational relationships are important [44].

Despite the increasing amount of related literature, 3-D face landmarking is still an open problem. Current face landmarking techniques lack both accuracy and robustness, particularly in the presence of lighting variations, head pose variations, scale changes, facial expressions, self-occlusions, and occlusion by accessories (e.g., hair, moustache, and eyeglasses) [1]. This paper proposes a data-driven general framework for precise 3-D face landmarking, which is robust to changes in facial expressions and partial occlusions.

Face landmarking on 2-D facial texture images has been extensively studied [1], and several approaches have been proposed. These approaches can be classified into appearance-based [2], geometry-based [3], and structure-based approaches [4], [5]. Interesting approaches include 2-D statistical models, such as the popular active appearance model [12] or the more recent constrained local model (CLM) [14], which perform statistical analysis both on the facial appearance and the 2-D shape. However, since they are applied to 2-D texture images, these approaches inherit the sensitivity to lighting and pose changes.

Manuscript received December 23, 2009; revised November 18, 2010, February 14, 2011, and March 29, 2011; accepted April 8, 2011. This work was supported in part by the French National Research Agency (ANR) through the ANR Omnia project under Grant ANR-07-MDCO-009-02 and through the ANR FAR 3-D project under Grant ANR-07-SESU-004-03. This paper was recommended by Associate Editor J. Su.

X. Zhao and I. A. Kakadiaris are with the Computational Biomedicine Laboratory, Department of Computer Science, University of Houston, Houston, TX 77204-3010 USA (e-mail: zhaoxi@ieee.org; ioannisk@uh.edu).

E. Dellandréa and L. Chen are with the Université de Lyon, Centre National de la Recherche Scientifique, Ecole Centrale Lyon, Laboratoire d'InfoRmatique en Image et Systèmes d'information, Unité Mixte de Recherche 5205, 69134 Ecully Cedex, France (e-mail: emmanuel.dellandrea@ec-lyon.fr; liming.chen@ec-lyon.fr).

Color versions of one or more of the figures in this paper are available online at <http://ieeexplore.ieee.org>.

Digital Object Identifier 10.1109/TSMCB.2011.2148711

74 Research on 3-D face landmarking is rather recent. Most of
 75 the existing methods embed *a priori* knowledge on landmarks
 76 on 3-D face by computing the response to local 3-D shape-
 77 related features (e.g., spin image [28], [42], [43], effective
 78 energy [10], Gabor filtering [7], [11], generalized Hough trans-
 79 form [24], local gradients [19], HK curvature [22], shape index
 80 [20], [42], [43], curviness index [21], and radial symmetry
 81 [29]). While these approaches enable a rather accurate detection
 82 of landmarks that are shape prominent (e.g., the nose tip or the
 83 inner corners of eyes), their localization accuracy drastically
 84 decreases for other less prominent landmarks.

85 As current 3-D imaging systems can deliver registered range
 86 and texture images, a straightforward method to discriminate a
 87 landmark is to accumulate evidence from both face representa-
 88 tions (i.e., face geometry and texture). Boehnen and Russ [27]
 89 computed the eye and mouth maps based on both color and
 90 range information. Wang *et al.* [25] used a “point signature”
 91 representation to code a 3-D face mesh as well as Gabor
 92 jets of landmarks from the 2-D texture image. Gabor wavelet
 93 coefficients [1], [23] were used to model the local appearance
 94 in the texture map and local shape in a range map around
 95 each landmark. Lu and Jain [32] proposed to compute and fuse
 96 the shape index response (range) and the cornerness response
 97 (texture) in local regions around seven feature points.

98 As the combinations of candidate landmarks resulting from
 99 shape and/or texture related descriptors are generally impor-
 100 tant, some studies also proposed to make use of the structure
 101 between landmarks. This is accomplished by using heuristics
 102 [21], a 3-D geometry-based confidence [27], an extended elastic
 103 bunch graph [23], or a simple mean model constructed as the
 104 average 3-D position of landmarks from a learning data set
 105 [30]. However, there is no technique that best takes into account
 106 both the configurational relationships between landmarks and
 107 the local properties in terms of geometric shape/texture around
 108 each landmark.

109 Furthermore, only few of the aforementioned studies address
 110 the issue of face landmarking in the presence of facial expres-
 111 sions or occlusions. Nair and Cavallaro [21] used their 3-D
 112 point distribution model (PDM) to locate five landmarks (the
 113 two outer eye points, the two inner eye points, and the nose
 114 tip) under facial expressions with a locating accuracy ranging
 115 from 8.83 mm for the nose tip to 20.46 mm for the right outer
 116 eye point. However, all the five landmarks were located on
 117 stable face regions during facial expressions. Dibeklioglu *et al.*
 118 [19] studied 3-D facial landmarking under expression, pose,
 119 and occlusion variations. They built statistical models of local
 120 features around landmark locations using a mixture of factor
 121 analysis in order to determine landmark locations on a coarse
 122 level. Heuristics were then applied to locate the nose tip at a
 123 fine level. Using the configurational relationships and geometry
 124 features, Perakis *et al.* [42], [43] addressed landmarking on
 125 3-D facial data under multiple orientations, taking into account
 126 missing data due to self occlusion.

127 B. Proposed Approach

128 In this paper, we propose a general learning-based framework
 129 for 3-D face landmarking which combines both configurational

relationships between the landmarks and their local properties 130
 in a principled way, through optimization of a global objective 131
 function. This data-driven based approach aims to overcome 132
 the shortcomings of the previous feature-based approaches that 133
 require the embedding of a discriminative prior knowledge for 134
 each landmark. Instead, it relies on a statistical model, called 135
 3-D Statistical Facial feAture Model (SFAM), which learns 136
 both the global variations in 3-D face morphology and the local 137
 variations around each 3-D face landmark in terms of texture 138
 and geometry. To train the model, we manually labeled the tar- 139
 get landmarks for each aligned frontal 3-D face. Preprocessing 140
 is first performed to enhance the quality of facial scans, and 141
 then, the scans are remeshed to normalize the face scale. The 142
 SFAM is then constructed by applying principle component 143
 analysis (PCA) to the global 3-D face landmark configurations, 144
 the local texture, and the local shape around each landmark 145
 from the training facial data. PCA-based learning is popular 146
 for face recognition since human faces are similar, and hence, 147
 it is quite reasonable to assume that the properties of facial 148
 features follow a Gaussian distribution, as demonstrated by 149
 previous studies (e.g., eigenfaces [45]). In our approach, only 150
 the salient variation modes (95% of the variation) for the 151
 three representations (morphology, texture, and geometry) are 152
 retained. By varying the control parameters of SFAM, different 153
 3-D partial face instances that consist of local face regions with 154
 texture and shape (structured by their global 3-D morphology) 155
 can be generated. In this paper, we have used a simple local 156
 range map and an intensity map to characterize the local shape 157
 and texture properties around each landmark. Alternatively, the 158
 SFAM may use all the aforementioned descriptors of local 159
 features around each landmark (e.g., mean and Gaussian curva- 160
 ture or shape index for local shape characterization and Gabor 161
 jets or cornerness response for local texture description). An 162
 interesting property for the characterization of the local shape 163
 around a landmark is that the descriptor is sufficiently robust 164
 against shape deformation, which typically occurs in facial 165
 expressions. Popular geometric descriptors (e.g., shape index or 166
 HK curvatures) provide an accurate local shape description and 167
 are sensitive to geometric shape differences. However, when the 168
 normalized correlation is used as the similarity measure, local 169
 shape properties described by raw range maps are less discrim- 170
 inative with respect to identity and deformations. Similarly, the 171
 description of local texture should be tolerant to changes caused 172
 by lighting or expressions. A similar reasoning also applies to 173
 using the raw texture maps for texture characterization. The 174
 combination of raw texture maps and the similarity measure 175
 relieves, to some extent, the effect of lighting conditions and 176
 expressions on texture. Our experiments indicate that the use 177
 of a local raw range map and a local raw texture map around 178
 each landmark provides a good tradeoff between computational 179
 efficiency and robustness. Although a comprehensive study of 180
 the selection of robust local features is needed, it is beyond the 181
 scope of this paper. 182

Our learning-based framework can be considered as a natural 183
 extension of the morphable 3-D face model [15] and the CLM 184
 [14] as we propose to learn, at the same time, the global vari- 185
 ations of 3-D face morphology and the local ones in terms of 186
 texture and shape around each landmark. Fitting the SFAM on 187

TABLE I
SUMMARY OF SYMBOLS

Symbols	Description
s	3D facial landmark configuration vector
g	Intensity vector
z	Geometry vector
ψ	SFAM
P	Learnt modes of variations
b	SFAM parameters
T	Texture map of a 3D facial scan
R	Range map of a 3D facial scan
m	Occlusion mask

188 a probe facial scan is accomplished by maximum *a posteriori*
 189 (MAP) probability. The fitted morphology instance delivers
 190 the locations of targeted landmarks. Using 3-D training faces
 191 with expressions, the SFAM has the ability to learn expression
 192 variations and generate instances with the learned variations
 193 so as to increase the *a posteriori* probability in fitting faces
 194 with expression. Furthermore, we propose to use a *k*-nearest
 195 neighbor (*k*-NN) classifier to identify the partially occluded
 196 faces and the type of occlusion. A histogram of the similarity
 197 map between the local shapes of the target face and shape
 198 instances from the SFAM is used as the input. This information
 199 about occlusions is also integrated into the objective function
 200 used in the fitting process to handle landmarking on partially
 201 occluded 3-D facial scans.

202 The main contributions of this paper are the following.

- 203 1) We build an SFAM that elegantly combines the global and
 204 local features extracted from three facial representations.
- 205 2) An occlusion detection and classification algorithm is
 206 proposed to detect occlusions and classify them into
 207 different types, thereby providing occlusion information
 208 to the fitting algorithm.
- 209 3) A fitting algorithm is proposed to locate landmarks
 210 through optimizing an objective function, implemented
 211 on local patch-based correlation meshes. In addition, the
 212 fitting algorithm incorporates occlusion knowledge and
 213 thus is able to locate landmarks on partially occluded
 214 faces.

215 The rest of this paper is organized as follows. In Section II,
 216 our statistical model SFAM is introduced. In Section III, the
 217 objective function that combines the local shape and texture
 218 properties and the fitting algorithm are described. Section IV
 219 addresses 3-D face partial occlusion. Experimental results are
 220 discussed in Section V, while Section VI concludes this paper.
 221 Table I presents a summary of the different symbols used in this
 222 paper.

223 II. SFAM

224 Three-dimensional facial data acquired by the current 3-D
 225 imaging systems are usually noisy and may contain holes and
 226 spikes. Hence, we first preprocess all the 3-D facial scans to
 227 remove noise. Head pose and scale variations are normalized by
 228 alignment and remeshing (see Section II-A). Then, we model
 229 the variations in 3-D configurations of landmarks and their
 230 local variations in terms of texture and shape around each
 231 landmark (see Section II-B). New partial 3-D face instances can
 232 be synthesized from the learned model (see Section II-C).

A. Preprocessing the Training Facial Data

233

To remove the noise (e.g., spikes and holes) and enhance
 the quality of 3-D facial scans, we perform the following
 operations.

- 1) Median cut: Spikes are detected by checking the discon-
 tinuity of points and are removed by the application of a
 median filter.
- 2) Hole filling: Holes that are caused by the 3-D scanner
 and the removed spikes are located on the range maps of
 facial scans by a morphological reconstruction [38] and
 filled by cubic interpolation. The open mouth is excluded
 from this preprocessing step by estimating the size of
 the hole corresponding to the open mouth region with an
 empirically set threshold.

Although faces are usually scanned from a frontal viewpoint,
 variations in head pose still exist and interfere with the learning
 of global variations in 3-D facial morphology. Consequently,
 these variations may perturb the learning of local shape and
 texture variations. To compensate for head pose variations,
 the facial data are first translated close to the origin of the
 coordinate system. The iterative closest point algorithm [18]
 is then used to minimize the difference between the two point
 clouds of the new scan and the selected facial scan, which
 holds a frontal and straight pose. Since the head pose variations
 have been compensated after alignment, the SFAM can be
 learned with more accurate variations in local face texture and
 geometry.

To train the model, the targeted anthropometric landmarks
 have to be manually labeled for each aligned frontal 3-D face.
 This is the major difference between the proposed approach and
 most of the existing 3-D face landmarking algorithms. Instead
 of directly embedding *a priori* knowledge on landmarks into
 the landmarking algorithm, we propose a data-driven approach
 which, through statistical learning, encodes into a model dis-
 criminatory information of targeted landmarks, in terms of their
 global configurational relationships as well as the properties
 of local texture and shape around each landmark. For any
 given training data set, the set of targeted landmarks can be
 easily changed according to the particular application. This
 general characteristic of the proposed approach is demonstrated
 in our experiments on three different public data sets: FRGC,
 BU-3-DFE, and Bosphorus data sets. Most landmarks out of 15
 (as illustrated in Fig. 5) on the FRGC data set were selected
 from the rigid part of the face as they were subsequently used
 for 3-D face recognition. On the other hand, landmarks on the
 BU-3-DFE and the Bosphorus data sets (as illustrated in Figs. 6
 and 8) encompass anthropometric points from all facial regions
 as they are used for facial expression analysis.

To learn the local geometry and texture around each land-
 mark, it is necessary to have the same number of points in a
 local region and have a dense correspondence among different
 faces. However, changes due to face scale and subject identity
 make this normalization difficult. Therefore, we use uniform
 grids to remesh local regions around landmarks. First, all the
 points are sampled from point clouds within a specified distance
 from each landmark. The number of sampled points, or the
 point density, in local regions varies from face to face due

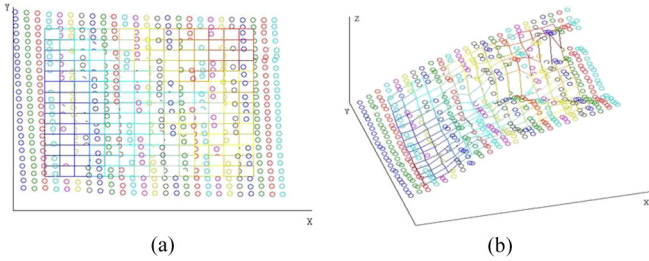


Fig. 1. Scale normalization in a local region associated to the left corner of the left eye from the (a) frontal view and (b) side view. Circles denote sampled points from the 3-D face model, and the grid is composed of the interpolated points. Interpolation is also performed on the point intensity values.

290 to face scale. Second, a uniform grid is associated with each
291 landmark. As illustrated in Fig. 1, each grid is centered at its
292 corresponding landmark with a size of 15×15 (225 nodes on a
293 grid) and a resolution of 1 mm (the intervals of grids on the X ,
294 Y dimensions are fixed to 1 mm). The z values of a node (and
295 the associated intensity values) on a grid are interpolated from
296 the range values of sampled points. Using this normalization, a
297 fixed number of points can be obtained regardless of face scale
298 and subject identity. Thus, the point-to-point correspondence
299 among faces is established easily and efficiently.

300 B. Modeling the Configurational Relationships and Local 301 Shape and Texture Features of the Landmarks

302 Once a 3-D facial scan is preprocessed, 3-D coordinates of all
303 the landmarks (3-D morphology) are concatenated into a vector
304 \mathbf{s}_i , which describes the configurational relationships among
305 local regions

$$\mathbf{s}_k = (x_1, y_1, z_1, x_2, y_2, z_2, \dots, x_N, y_N, z_N)^T \quad (1)$$

306 where N is the number of landmarks (e.g., in this paper, $N =$
307 15 or 19).

308 We further generate the two vectors \mathbf{g}_k and \mathbf{z}_k by concate-
309 nating intensity and range values on all the grids on a face
310 (M is the number of interpolated points collected from all the
311 local regions). The \mathbf{z}_k vectors capture the variations of local
312 geometric shapes around each landmark while the \mathbf{g}_k vectors
313 capture the local texture properties

$$\mathbf{g}_k = (g_1^k, g_2^k, \dots, g_M^k)^T, \quad \mathbf{z}_k = (z_1^k, z_2^k, \dots, z_M^k)^T. \quad (2)$$

314 PCA is then applied to the three vector sets $\{\mathbf{s}_k\}$, $\{\mathbf{g}_k\}$, and
315 $\{\mathbf{z}_k\}$, extracted from the training 3-D facial data (k denotes
316 the k th training example). Thus, three linear models are built
317 by retaining 95% of the variance in landmark configurations as
318 well as local texture and shape around each landmark. The three
319 models are represented as follows:

$$\mathbf{s} = \bar{\mathbf{s}} + \mathbf{P}_s \mathbf{b}_s \quad (3)$$

$$\mathbf{g} = \bar{\mathbf{g}} + \mathbf{P}_g \mathbf{b}_g, \quad \mathbf{z} = \bar{\mathbf{z}} + \mathbf{P}_z \mathbf{b}_z \quad (4)$$

320 where $\bar{\mathbf{s}}$, $\bar{\mathbf{g}}$, and $\bar{\mathbf{z}}$ are the mean landmark configuration, the
321 mean intensity, and the mean range value, respectively, while

\mathbf{P}_s , \mathbf{P}_g , and \mathbf{P}_z are the three sets of modes of configuration, 322
intensity, and depth variation, respectively. The terms \mathbf{b}_s , \mathbf{b}_g , 323
and \mathbf{b}_z are the corresponding sets of control parameters. All 324
individual components in \mathbf{b}_s , \mathbf{b}_g , and \mathbf{b}_z are independent. 325
We further assume that all the \mathbf{b}_q -parameters, where $\mathbf{b}_q \in$ 326
($\mathbf{b}_s, \mathbf{b}_g, \mathbf{b}_z$), follow a Gaussian distribution with zero mean and 327
standard deviation σ_q . 328

C. Synthesizing Instances From a New Face

329
330 Given the parameters \mathbf{b}_s , a configuration instance can be
331 generated using (3). Then, given a new facial scan, the set of
332 scan points closest to the configuration instance is computed.
333 Based on these points, the vectors \mathbf{g}^n and \mathbf{z}^n are obtained by
334 applying the process described in the training phase (2). Then,
335 \mathbf{b}_g and \mathbf{b}_z are estimated as follows:

$$\mathbf{b}_g = \mathbf{P}_g^T (\mathbf{g}^n - \bar{\mathbf{g}}), \quad \mathbf{b}_z = \mathbf{P}_z^T (\mathbf{z}^n - \bar{\mathbf{z}}). \quad (5)$$

\mathbf{b}_g and \mathbf{b}_z are limited to the range $[-3\sigma, 3\sigma]$. Then, using 336
these constrained \mathbf{b}_g and \mathbf{b}_z , we can generate texture and shape 337
instances $\hat{\mathbf{g}}^n$ and $\hat{\mathbf{z}}^n$ by using (4). The landmarks, along with 338
their local texture and local shape instances, compose a partial 339
face instance. 340

III. LOCALIZING LANDMARKS

341
342 The SFAM-based landmark localization procedure consists
343 of MAP probability of landmark configuration, given a 3-D
344 facial scan to be landmarked, and leads to optimizing an
345 objective function. In Section III-A, we present the objective
346 function to be optimized, and in Section III-B, we introduce the
347 fitting algorithm for localizing landmarks. We then discuss our
348 assumptions in Section III-C.

A. Objective Function and MAP

349
350 We first define the objective function $f(\mathbf{b}_s) = p(\mathbf{s}|T, R, \psi)$
351 as the *a posteriori* probability of landmark configuration \mathbf{s} to be
352 maximized for a 3-D facial scan represented by its texture map
353 T and range map R and the learned statistical model SFAM ψ .
354 Using the Bayes rule, we obtain

$$\begin{aligned} p(\mathbf{s}|T, R, \psi) &= p(T, R, \mathbf{s}, \psi) / p(T, R, \psi) \\ &\propto p(T, R|\mathbf{s}, \psi) p(\mathbf{s}|\psi) \\ &\propto p(T|\mathbf{s}, \psi) p(R|\mathbf{s}, \psi) p(\mathbf{s}|\psi) \end{aligned} \quad (6)$$

355 where $p(T|\mathbf{s}, \psi)$ and $p(R|\mathbf{s}, \psi)$ are the probabilities of having
356 the facial texture T and the range R , given a landmark configu-
357 ration \mathbf{s} and SFAM ψ , respectively. We assume that the random
358 variables R and T from the different facial representations
359 are independent within a local face region. The term $p(\mathbf{s}|\psi)$
360 denotes the probability of having a landmark configuration \mathbf{s}
361 given the SFAM ψ . Thus, the prior $p(\mathbf{s}|\psi)$ can be estimated
362 using the assumption of Gaussian distribution on the corre-
363 sponding control parameters \mathbf{b}_j in the third term of (7).

364 The probabilities $p(T|s, \psi)$ and $p(R|s, \psi)$ can be estimated
 365 using the Gibbs–Boltzmann distribution as described in

$$p(\mathbf{s}|T, R, \psi) \propto \prod_{i=1}^N e^{-(\alpha\eta_i)} \prod_{i=1}^N e^{-(\beta\gamma_i)} \prod_{j=1}^K e^{-\frac{b_j^2}{\lambda_j}}$$

$$\log p(\mathbf{s}|T, R, \psi) \propto \sum_{i=1}^N (-\alpha\eta_i) + \sum_{i=1}^N (-\beta\gamma_i) - \sum_{j=1}^K \frac{b_j^2}{\lambda_j} \quad (7)$$

366 where N is the number of local regions, η_i and γ_i are the energy
 367 functions of the associated local region i in terms of texture and
 368 range properties, respectively, given the landmark configuration
 369 \mathbf{s} and the SFAM ψ , and α and β are weight constants. The
 370 third term in (7) represents the Mahalanobis distance [13],
 371 where K is the number of retained landmark configuration
 372 modes and λ_j denotes the corresponding eigenvalue in the
 373 landmark configuration model. b_j denotes the control parameter
 374 that generates the landmark configuration \mathbf{s} given the statistical
 375 model ψ . For the energy functions η_i and γ_i , high energies
 376 occur when the corresponding local texture T_i and range R_i do
 377 not match the texture and range instances which are generated
 378 by the SFAM ψ given the landmark configuration \mathbf{s} . In this
 379 paper, instead of using the distances in these energy functions
 380 to express the degree of mismatch, we use a similarity measure,
 381 namely, the normalized correlations defined in (9), and derive
 382 the following objective function $f(\mathbf{b}_s)$ (thereby changing the
 383 polarity of the terms associated with η_i and γ_i):

$$f(\mathbf{b}_s) = \alpha \sum_{i=1}^N m_i F_{gi}(s_i) + \beta \sum_{i=1}^N m_i F_{zi}(s_i) - \sum_{j=1}^k \frac{b_j^2}{\lambda_j} \quad (8)$$

384 where F_{gi} and F_{zi} are explained in (9) and m_i is introduced
 385 to address partially occluded facial data. The term m_i is the
 386 probability of the region around the i th landmark being un-
 387 occluded. The term s_i denotes the landmark location from the
 388 morphology model. Specifically

$$F_{gi} = \left\langle \frac{\mathbf{g}_i}{\|\mathbf{g}_i\|}, \frac{\hat{\mathbf{g}}_i}{\|\hat{\mathbf{g}}_i\|} \right\rangle \quad F_{zi} = \left\langle \frac{\mathbf{z}_i}{\|\mathbf{z}_i\|}, \frac{\hat{\mathbf{z}}_i}{\|\hat{\mathbf{z}}_i\|} \right\rangle \quad (9)$$

389 where $\langle \cdot, \cdot \rangle$ is the inner product and $\|\cdot\|$ is the L_2 norm. The
 390 values of α and β are fixed and are computed as the ratios
 391 of $\sum_{i=1}^N F_{gi}$ and $\sum_{j=1}^K (b_j^2/\lambda_j)$, $\sum_{i=1}^N F_{zi}$, and $\sum_{j=1}^K (b_j^2/\lambda_j)$,
 392 respectively, during the offline training.

393 In this paper, we have used a simple occlusion classification
 394 algorithm which delivers a binary value for m_i : zero if the local
 395 region is occluded and one if the region is not occluded.

396 B. Fitting Algorithm

397 Landmarking a 3-D facial scan consists of fitting the SFAM
 398 ψ while maximizing the objective function (8). First, the 3-
 399 D facial scan is preprocessed as described in Section II-A,
 400 including spike removal, hole filling, and head pose normal-
 401 ization. The occlusion algorithm, introduced in Section IV, is
 402 then applied to identify the occluded local regions and then
 403 used to set the corresponding m_i coefficients to zero. Therefore,
 404 only the unoccluded local regions are considered in the fitting
 405 process. The algorithm works in a straightforward manner and
 406 is described in Algorithm 1.

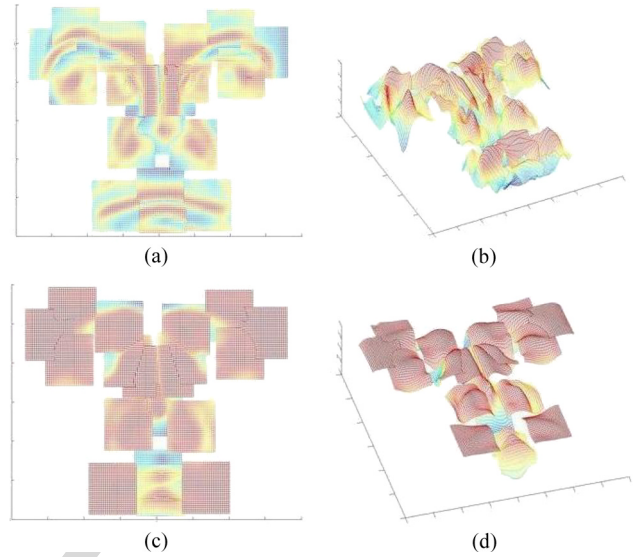


Fig. 2. Depiction of the correlation meshes from the frontal and side views. These meshes capture the similarity between instances and local facial regions in both texture and shape representations. The red color corresponds to large correlation values while blue corresponds to small correlation values. Large values on the correlation meshes correspond to large probabilities of finding landmarks on their locations. The meshes are in four-dimensional space, where the first three dimensions are x , y , z and the last dimension represents correlation values. In these figures, we display the correlation values instead of z . (a,b) Two viewpoints of the same correlation mesh capturing the similarity of texture (intensity) instances from SFAM and local texture regions (intensity) on a given face. (c,d) Correlation mesh capturing the similarity of shape (range) instances from SFAM and the local face shapes (range).

Algorithm 1 SFAM Fitting

Input: A 3-D scan and a trained SFAM.

1. Optimize the morphology parameters \mathbf{b}_s to minimize the distance between corresponding morphology instances and their closest points on the input facial data, and obtain a set of points \mathcal{S} .
 2. Synthesize texture and shape instances \hat{G} , \hat{Z} as described in Section II-C using \mathcal{S} .
 3. Normalize local regions around points \mathcal{S} within a neighborhood large enough to cover the potential landmark locations as in Section II-A, creating a set of local mesh \mathcal{G} , \mathcal{Z} .
 4. Compute correlation meshes on both texture and geometry representations (see Fig. 2) by correlating \hat{G} , \hat{Z} with G , Z , respectively, which are different parts of \mathcal{G} , \mathcal{Z} sampled by a sliding window (size of 15×15) on local regions (9).
 5. Optimize the morphology parameters \mathbf{b}_s to reach the maximum of the sum of values on the two correlation meshes while minimizing the Mahalanobis distance associated with the landmark configuration defined by the control parameters \mathbf{b}_s .
- Output:** Optimized morphology parameters \mathbf{b}_s .

The optimization process in steps one and five of the algorithm is processed by the Nelder–Mead simplex algorithm [16]. Once convergence is reached, the instance \mathbf{s} resulting from the optimized \mathbf{b}_s indicates the location of landmarks. For partially occluded faces, occluded landmarks and their corresponding local meshes are excluded from the optimization process. In the case of incorrect occlusion classification, local nonface meshes lead the optimization to converge to an unpredictable point far from the desired minimum.

436 C. Discussion

437 To deduce (7), we assumed that the probabilities $p(T|s, \psi)$
 438 and $p(R|s, \psi)$ follow a Gibbs–Boltzmann distribution. This
 439 assumption is reasonable and motivated by the fact that the
 440 problem of 3-D face landmarking is actually a Markov random
 441 field (MRF) which consists of assigning a label from a set of
 442 labels \mathcal{L} to each vertex of a 3-D facial scan. The set \mathcal{L} encom-
 443 passes all targeted landmarks (e.g., nose tip and eye corners)
 444 and a null value labeling any vertex which is not the location
 445 of a targeted landmark. Then, the theorem of the equivalence
 446 between MRFs and Gibbs distributions defined by Hammersley
 447 and Clifford [39] implies that the probabilities $p(T|s, \psi)$ and
 448 $p(R|s, \psi)$ follow a Gibbs–Boltzmann distribution [40].

449 We also used the Nelder–Mead simplex algorithm [16],
 450 which is one of the best known algorithms for multidimensional
 451 unconstrained optimization without derivatives. This method
 452 does not require any derivative information and is widely used
 453 to solve parameter estimation and statistical problems of similar
 454 nature [41].

455 IV. OCCLUSION DETECTION AND CLASSIFICATION

456 Facial data analysis in the presence of partial occlusions
 457 (caused by a variety of factors such as hair, glasses, mustaches,
 458 and scarf) is a difficult problem. In 3-D facial landmarking, only
 459 occlusions which may occur in local regions around landmarks
 460 are of interest. Thus, in this paper, we adopt an approach to
 461 classify the occlusion type and provide a set of binary values to
 462 local regions: either occluded or not occluded. Alternatively, we
 463 may compute a probability associated with a local region being
 464 occluded or a measure indicating roughly the extent to which a
 465 local region is occluded.

466 To perform occlusion detection, features from the range map
 467 are extracted as the presence of occlusion definitively changes
 468 local shape. Therefore, given a new facial scan, its closest points
 469 to the mean landmark configuration $\bar{s}(3)$ are first computed.
 470 Then, grids (50×50) are used to remesh local regions around
 471 these points for range values (see Section II-A). The size of
 472 local regions is chosen to be large enough to account for
 473 variations due to scale and subject changes as well as to cover
 474 the local regions near landmarks for occlusion detection.

475 For each local region i , processing is performed in a sliding
 476 window manner (the size of the sliding window is the same as
 477 the size of the local regions considered in the SFAM). At each
 478 step, we compute a local depth map Z_α and its local shape
 479 instance Z_β to further obtain a similarity L_S as follows:

$$b_{alpha} = P_{z,i}^T(Z_\alpha - \bar{z}_i), Z_\beta = \bar{z}_i + P_{z,i}b_\beta \quad (10)$$

$$L_S = \left\langle \frac{Z_\alpha}{\|Z_\alpha\|}, \frac{Z_\beta}{\|Z_\beta\|} \right\rangle \quad (11)$$

480 where $P_{z,i}$ is the submatrix composed of the rows in P_z
 481 associated with local region i . The term \bar{z}_i is the subvector
 482 composed of the rows in \bar{z} also associated with local region i .
 483 The term b_β is obtained by limiting b_α within the boundary as
 484 described in Section II-C. In the case of occlusion, b_α does not
 485 necessarily obey a Gaussian distribution and may be distributed

far away from the mean value. Thus, by boundary limitation, the
 instances Z_β are different from the occluded local shape Z_α ,
 leading to a low similarity value in (11).

The local similarity value L_S is computed for all points in
 a local region, leading to a local similarity map. We then build
 a histogram of L_S values using 50 bins to represent the values
 ranging from -1 to 1 . Since most values in the local similarity
 map are close to 1 , we allocate more bins near 1 . Then, the his-
 tograms computed from all the local regions are concatenated
 into a single feature vector. Partially occluded 3-D facial scans
 in the training set are manually labeled according to a given
 occlusion type (i.e., occlusion in the ocular region, occlusion
 in the mouth region, occlusion by glasses, or unoccluded). The
 distance between histograms is computed using the Euclidean
 metric, and the classification is performed using a simple k -NN
 classifier.

In our experiments, we used the Bosphorus data set which
 encompasses partially occluded 3-D facial scans according to
 several occlusion patterns. We preset a set of binary values
 indicating the occlusion state in each local region for each
 occlusion pattern. By classifying facial scans into these states,
 we can thus obtain a list of local regions that are occluded
 $[m_i$ in (8)].

V. EXPERIMENTAL RESULTS

The proposed statistical learning-based framework for 3-D
 facial landmarking was applied on three data sets, namely, the
 FRGC [35], BU-3-DFE [36], and Bosphorus [37] data sets. In
 Section V-A, we describe the data sets and the experimental
 setup and present the various experimental results in the follow-
 ing sections. These results are further discussed in Section V-E.

A. Data Sets and Experimental Setup

The FRGC data set includes two versions. FRGC v1 con-
 tains 953 scans from 275 people, captured under controlled
 illumination conditions and generally neutral expressions [35].
 However, these 953 facial scans have slight head pose and scale
 variation. In addition, FRGC v1 contains 33 noisy 3-D facial
 scans having uncorrected correspondence between the range
 and texture maps. These scans were not used in our experi-
 ment. FRGC v2 contains 4007 facial scans from 466 persons.
 These 3-D facial scans were captured under different illumina-
 tion conditions and contain various facial expressions (such as
 happiness or surprise).

The BU-3-DFE database contains data from 100 subjects
 [36]. Each subject performed a neutral expression and six uni-
 versal expressions in front of a 3-D scanner. Each of these six
 universal expressions (happiness, disgust, fear, anger, surprise,
 and sadness) is displayed with four levels of intensity. In our
 experiments, we have used the neutral facial data and facial data
 with expressions in the two high-level intensities from all the
 subjects, resulting in 1300 facial scans in total.

The Bosphorus data set contains 3396 facial scans from 104
 subjects [37]. This data set contains not only the six universal
 facial expressions but also 3-D scans under realistic occlusions
 (e.g., glasses, hands around the mouth, and eye rubbing).

TABLE II
CONFUSION MATRIX OF OCCLUSION CLASSIFICATION

	Eye	Mouth	Glass	Unoccluded
Eye	93.3 %	2.2 %	2.4 %	2.1 %
Mouth	1.0 %	97.4 %	1.6 %	0.0 %
Glass	7.3 %	3.3 %	84.4 %	4.5 %
Unoccluded	0.0 %	0.0 %	0.0 %	100.0 %

540 Moreover, the data set includes many male subjects that have
541 moustache and beard.

542 As illustrated in Figs. 5–8, we manually labeled 15 facial
543 landmarks in the FRGC data set and used 19 labeled landmarks
544 in the BU-3-DFE and Bosphorus data sets. They were used
545 as ground truth for learning the SFAM model and testing our
546 landmark fitting algorithm. These three landmark data sets
547 contain some common landmarks, such as eye corners and
548 mouth corners, which are sensitive to facial expressions.

549 B. Occlusion Classification Results

550 The proposed algorithm for occlusion detection was applied
551 to 3-D scans from the Bosphorus data set. In our experiment,
552 we excluded partial occlusions by hair as they do not occur in
553 the landmark regions. We have considered partial occlusions
554 caused by glasses, a hand near the mouth region, and a hand
555 near the ocular region in addition to unoccluded 3-D scans.
556 We experimentally set k to five in the k -NN classifier and
557 performed a two-fold cross-validation. The confusion matrix
558 is provided in Table II. An average classification accuracy up
559 to 93.8% is achieved, which appears to be sufficient for the
560 subsequent landmarking task.

561 C. Results on SFAM

562 We used 452 scans from the FRGC v1 data set to build
563 the SFAM-1 model by learning the local properties around
564 15 landmarks and their configurational relationships. The train-
565 ing facial scans have limited illumination variations and do not
566 contain facial expressions.

567 Furthermore, we used facial scans from 11 subjects in the
568 BU-3-DFE data set and the first 32 subjects in the Bosphorus
569 data set to build the SFAM-2 and SFAM-3, respectively. For
570 every subject, 13 scans were used for training in the case of
571 the BU-3-DFE data set (a neutral scan and the two scans for
572 each of the six universal expressions at the intensity levels three
573 and four), and seven scans in the case of the Bosphorus data
574 set (a neutral scan and a scan for each of the six universal
575 expressions). Fig. 3 illustrates the SFAM-3 learned from the
576 Bosphorus data set containing the first mode of configuration,
577 local texture, and local shape for variances $3 \pm \sigma$.

578 D. Results on Landmarking

579 Using the learned statistical models, the fitting algorithm
580 for 3-D face landmarking was evaluated on three different
581 experimental setups. In all these experiments, the errors were
582 computed as the Euclidean distance between the automatically
583 localized and the corresponding manually labeled landmarks.

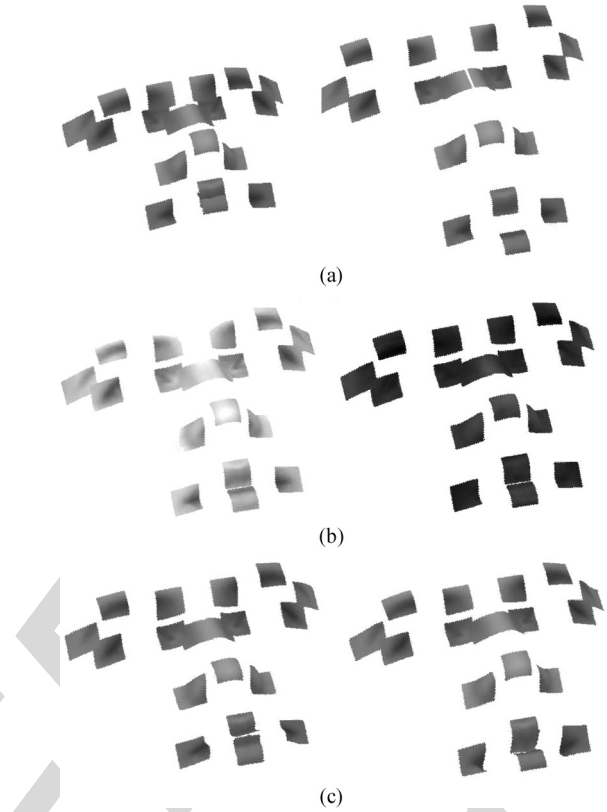


Fig. 3. SFAM learned from the Bosphorus data set. (a) First landmark configuration mode explains variations in terms of the face size and expression. (b) First texture mode explains skin color variations. (c) First range mode explains surface geometry variations, mainly in the nose and mouth regions.

Using the SFAM-1, the fitting algorithm was first applied on
584 the remaining FRGC v1 data sets (i.e., 462 scans from subjects
585 different from those in training). We then tested the algorithm
586 on 1500 facial scans (randomly selected from the FRGC v2 data
587 set) which contain illumination variations and facial expres-
588 sions. Fig. 4 depicts the cumulative distribution of the fitting
589 error for all 15 landmarks. Note that most landmarks were
590 automatically localized within 9 mm in both tests. Table III
591 summarizes the mean, the standard deviation of localization
592 errors associated with each landmark tested on FRGC v1 and
593 FRGC v2, and a comparison with the result achieved by a
594 curvature-analysis-based landmarking method [31]. The first
595 two columns show the mean and the standard deviation of lo-
596 calization error for each landmark (d_i) from our method while
597 the third column depicts the results achieved by the curvature-
598 analysis-based method. Note that the mean localization error
599 of all landmarks is less than 5 mm. An increase in the mean
600 and the standard deviation of errors generated in the experiment
601 on FRGC v2 compared with FRGC v1 was mainly caused by
602 uncontrolled illumination and facial expressions on tested facial
603 scans. Compared to curvature-analysis-based method, which
604 only uses geometry knowledge on faces, the proposed approach
605 can locate a larger number of landmarks. The mean and stan-
606 dard deviation in localization errors from our method were
607 smaller when compared to those obtained from the curvature-
608 analysis-based method except for the nose tip, which is the
609 most shape salient landmark on a face. Fig. 5 illustrates selected
610 landmark localization results from the first two experiments. 611

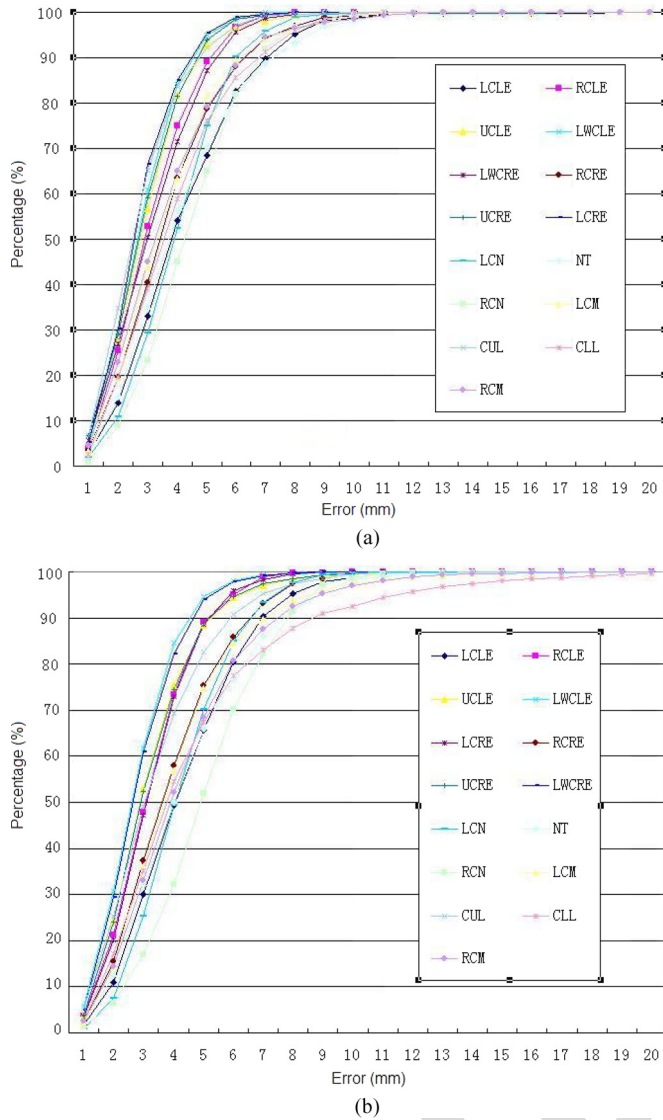


Fig. 4. Cumulative error distribution of the error for the 15 landmarks using (a) FRGC v1 and (b) FRGC v2. The symbols used are the following: LCLE—left corner of left eye, RCLE—right corner of left eye, UCLE—upper corner of left eye, LWCLE—lower corner of left eye, LCRE—left corner of right eye, RCRE—right corner of right eye, UCRE—upper corner of right eye, LWCRE—lower corner of right eye, LCN—left corner of nose, NT—nose tip, RCN—right corner of nose, LCM—left corner of mouth, CUL—center of upper lip, CLL—center of lower lip, and RCM—right corner of mouth.

The third experiment was carried out on the BU-3-DFE data set. Recall that 143 facial scans from the first five male subjects and six female subjects were used for training the SFAM-2. From the remaining 89 subjects, 1157 facial scans in total were used for testing. Each tested subject has a neutral expression and the six universal facial expressions at the intensity levels three and four. Fig. 6 illustrates several localization examples having facial expressions. Fig. 7 depicts the effect of expressions on landmarking accuracy. Note that landmarks with less deformation in expressions were better localized (i.e., eye corner, nose tip, and nose corner). Mouth corners and the middle of the lower lip were detected with the worst accuracy, and the largest standard deviation was observed in scans displaying surprise because of the large mouth displacement and ample deformation in this region. Table IV summarizes

TABLE III
COMPARISON OF MEAN ERROR AND STANDARD DEVIATION ASSOCIATED WITH EACH OF THE 15 LANDMARKS ON THE FRGC DATA SET

ID	Mean (std) <i>mm</i>		
	I	II	III
LCLE	4.17 (2.13)	4.31 (2.05)	7.87 (4.06)
RCLE	3.07 (1.42)	3.21 (1.44)	3.68 (1.98)
UCLE	2.92 (1.39)	3.17 (1.66)	- (-)
LWCLE	2.76 (1.21)	2.75 (1.31)	- (-)
LCRE	3.15 (1.56)	3.24 (1.43)	3.75 (1.96)
RCRE	3.67 (1.90)	3.89 (2.04)	6.59 (3.42)
UCRE	2.84 (1.45)	3.18 (1.63)	- (-)
LWCRE	2.68 (1.21)	2.83 (1.38)	- (-)
LSN	3.96 (1.65)	4.21 (1.71)	6.50 (5.36)
NT	4.11 (2.20)	4.43 (2.56)	1.93 (1.16)
RSN	4.39 (1.85)	5.07 (2.36)	6.81 (5.31)
LCM	3.61 (1.92)	4.09 (2.32)	9.10 (7.58)
CUL	2.74 (1.42)	3.37 (1.89)	- (-)
CLL	3.81 (1.97)	4.65 (3.41)	- (-)
RCM	3.58 (1.99)	4.34 (2.50)	8.83 (7.59)

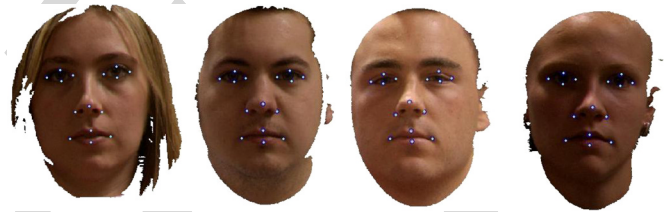


Fig. 5. Landmark localization examples from the FRGC data set.

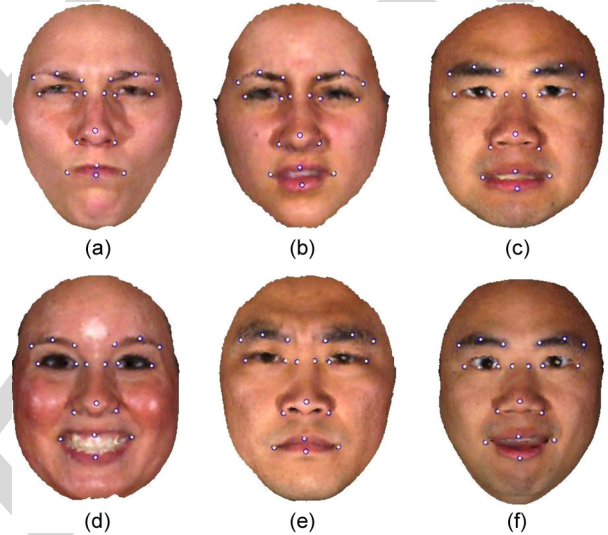


Fig. 6. Landmarking examples from the BU-3-DFE data set with expressions. (a) Anger. (b) Disgust. (c) Fear. (d) Happiness. (e) Sadness. (f) Surprise.

the mean error and the standard deviation of the proposed landmarking algorithm compared to the mean error of a PDM [21], which is trained with 150 face scans and tested on the remainder of the BU-3-DFE data set. Because of the use of local texture and geometry knowledge in our approach, there is a significant decrease in the localization errors. The mean error for all 19 landmarks is within 10 mm while most of standard deviations are lower than 5 mm. The localization accuracy of landmarks in the rigid face region is comparable to those of the corresponding landmarks automatically localized in FRGC.

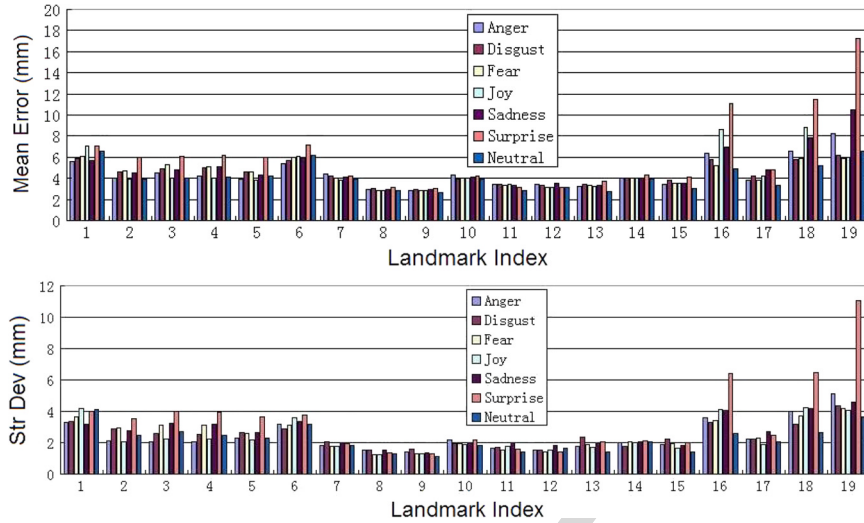


Fig. 7. Landmarking accuracy on different expressions with the BU-3-DFE data set. 1: Left corner of left eyebrow. 2: Middle of left eyebrow. 3: Right corner of left eyebrow. 4: Left corner of right eyebrow. 5: Middle of left eyebrow. 6: Right corner of right eyebrow. 7: Left corner of left eye. 8: Right corner of left eye. 9: Left corner of right eye. 10: Right corner of right eye. 11: Left nose saddle. 12: Right nose saddle. 13: Left corner of nose. 14: Nose tip. 15: Right corner of nose. 16: Left corner of mouth. 17: Middle of upper lip. 18: Right corner of mouth. 19: Middle of lower lip.

TABLE IV
MEAN ERROR AND THE CORRESPONDING STANDARD DEVIATION (IN MILLIMETERS) OF THE 19 AUTOMATICALLY LOCALIZED LANDMARKS ON THE FACIAL SCANS FROM THE BU-3-DFE DATA SET (ALL EXPRESSIONS INCLUDED)

ID	Mean	Std	Mean	ID	Mean	Std	Mean
1	6.26	3.72	-	11	3.30	1.70	-
2	4.58	2.82	-	12	3.27	1.56	-
3	4.87	2.99	-	13	3.32	1.94	-
4	4.88	2.97	-	14	4.04	1.99	8.83
5	4.51	2.77	-	15	3.62	1.91	-
6	6.07	3.35	-	16	7.15	4.64	-
7	4.11	1.89	20.46	17	4.19	2.34	-
8	2.93	1.40	12.11	18	7.52	4.75	-
9	2.90	1.36	11.89	19	8.82	7.12	-
10	4.07	2.00	19.38				

TABLE V
MEAN ERROR AND THE CORRESPONDING STANDARD DEVIATION ASSOCIATED WITH EACH OF THE 19 AUTOMATICALLY LOCALIZED LANDMARKS ON THE FACIAL SCANS FROM THE BOSPHORUS DATA SET UNDER OCCLUSION

ID	Mean (Std) <i>mm</i>		ID	Mean (Std) <i>mm</i>	
	I	II		I	II
1	9.66 (6.08)	11.95 (8.85)	11	7.50 (3.60)	7.56 (3.88)
2	8.29 (3.92)	8.47 (4.39)	12	7.58 (3.63)	6.92 (4.02)
3	7.33 (3.41)	7.15 (3.36)	13	6.35 (3.11)	7.19 (2.99)
4	7.02 (3.23)	6.77 (3.38)	14	8.46 (3.64)	8.39 (3.64)
5	8.21 (4.27)	8.20 (4.45)	15	8.03 (3.31)	7.79 (3.36)
6	9.74 (5.23)	10.05 (6.08)	16	7.96 (4.18)	9.75 (6.28)
7	7.01 (3.77)	8.83 (6.37)	17	8.67 (4.84)	9.01 (4.93)
8	6.25 (3.42)	6.87 (4.21)	18	8.21 (4.25)	9.65 (4.97)
9	6.44 (3.08)	6.51 (3.58)	19	10.41 (5.37)	10.61 (5.61)
10	7.46 (3.56)	7.86 (4.73)			

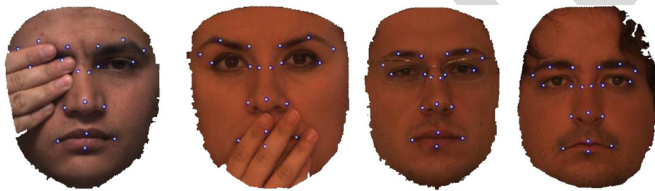


Fig. 8. Landmarking examples from the Bosphorus data set with occlusion. From left to right, faces are occluded in the eye region, in the mouth region, by glasses, and by hair.

637 The last experiment tested the fitting algorithm using the
 638 SFAM-3 to locate 19 landmarks on 3-D scans under occlusion
 639 from the Bosphorus data set. Fig. 8 illustrates several localiza-
 640 tion examples under occlusion. This experiment was carried out
 641 on 292 scans from all the subjects excluding the ones used for
 642 training in the Bosphorus data set. To evaluate the efficiency of
 643 our proposed occlusion classifier, the fitting algorithm was first
 644 tested with occlusion knowledge directly provided by the data
 645 set and, then, with occlusion knowledge from our occlusion
 646 detection and classification algorithm (see Table V). In both
 647 configurations, the mean errors ranged from 6 to 11 mm.
 648 Meanwhile, 71.4% of the landmarks were localized with a 10-

mm precision, and 97% of the landmarks were located with a 649
 20-mm precision. Note that there is only a slight increase on 650
 mean error and standard deviation on average when we switch 651
 the accurate knowledge on occlusion as provided by the data 652
 set to the one provided by the proposed occlusion detection 653
 algorithm described in Section IV. 654

E. Discussion

655

We studied the influence of landmark configuration on the 656
 landmarking results (see Table VI). Three sets of landmarks, 657
 consisting of 5, 9, and 15 landmarks, respectively, were tested 658
 on 100 facial scans randomly selected from the FRGC v1 data 659
 set. The subjects depicted in these scans were different from 660
 the subjects used for training the SFAM, which is the SFAM-1 661
 described in Section V-C. From Table VI, it is evident that the 662
 mean errors remain stable (with a slight decrease in some cases) 663
 when the number of landmarks increases from 5 to 15. Mean- 664
 while, there exists an upper bound on the number of landmarks, 665
 which depends upon the distinctiveness of landmarks so far 666
 characterized in this paper based on their global configurational 667

TABLE VI
INFLUENCE OF LANDMARK CONFIGURATION
ON MEAN ERRORS (IN MILLIMETERS)

	Mean(Std) <i>mm</i>		
	I	II	III
LCLÉ	- (-)	4.96 (2.33)	4.79 (2.15)
RCLÉ	3.20 (1.73)	3.15 (1.70)	3.14 (1.70)
UCLÉ	- (-)	- (-)	2.74 (1.30)
LWCLE	- (-)	- (-)	2.46 (1.32)
LCRE	3.60 (1.61)	3.56 (1.63)	3.56 (1.61)
RCRE	- (-)	3.73 (1.77)	3.57 (1.55)
UCRE	- (-)	- (-)	2.66 (1.08)
LWCRE	- (-)	- (-)	2.49 (1.15)
LSn	- (-)	3.92 (1.51)	3.91 (1.52)
NT	4.72 (2.58)	4.46 (2.63)	4.67 (2.51)
RSN	- (-)	4.55 (2.01)	4.41 (2.19)
LCM	3.89 (2.57)	4.07 (2.54)	3.89 (2.57)
CUL	- (-)	- (-)	2.70 (1.62)
CLL	- (-)	- (-)	4.10 (2.18)
RCM	3.77 (2.55)	3.71 (2.55)	3.75 (2.56)

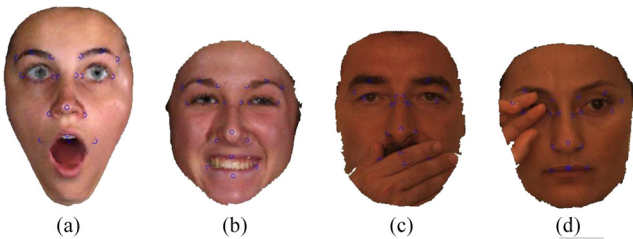


Fig. 9. Selected examples of failure cases. Facial data with (a) surprise, (b) happiness, (c) occlusion in mouth region, and (d) occlusion in eye region.

relationships and their local properties in terms of texture and geometric shape.

The computation time of the proposed algorithm for localizing landmarks on a scan (coded in Matlab) is around 10 min on a desktop PC with Intel Core i7-870 CPU and 8-GB RAM. The time consumed in Step 1 of the fitting algorithm is 130 s on average. It takes 70 to 96 s to compute the correlation meshes in Step 4, depending on the density of the point clouds. The computation time for the optimization of the objective function mainly depends on the speed of convergence. Over 99% of the cases converge within 2000 iterations or 422 s on average.

Fig. 9 illustrates several failure cases of landmarking under different conditions. Cases (a) and (b) are mainly due to ample deformation on the mouth region when faces display exaggerated expressions. The morphology model in the SFAM learns major variation modes from a mixture of expressions and subject identities and does not contain a specific mode for deformation caused by a specific facial expression. When fitting an SFAM on a facial scan having exaggerated facial morphology deformation (e.g., when displaying happiness and surprise), the fitting algorithm sometimes cannot generate morphology instances which approximate these extreme deformations in the mouth region. Cases (c) and (d) are mainly due to information loss in the fitting process when occlusion occurs. The occluded local regions are excluded in the fitting algorithm. Thus, the prediction of morphology parameters uses less information and is not as accurate and robust to local minima as the prediction when there is no occlusion.

We also studied the reproducibility and the corresponding accuracy of manual landmarking. For this purpose, 11 subjects were asked to manually label the 15 landmarks as defined in Fig. 5 on the same 10 facial scans randomly selected from FRGC v1. We then computed the mean error and the corresponding standard deviation of these manually labeled landmarks based on their mean landmark positions. The mean error of these manually labeled 15 landmarks was 2.49 mm with the associated standard deviation at 1.34 mm. In comparison, our localization technique achieved a mean error of 3.43 mm with the corresponding standard deviation of 1.68 mm on the same data set.

Compared to previous 3-D face landmarking algorithms [7], [8], [10], [17], [19], [21], [31], [32], our SFAM-based algorithm is a general data-driven 3-D landmarking framework which encodes the configurational relationships of the landmarks and their local properties in terms of texture and shape by a statistical learning approach instead of using heuristics directly embedded within the algorithm. Thus, our algorithm is more flexible and enables localizing landmarks which are not necessarily shape prominent or texture salient.

VI. CONCLUSION

In this paper, we have presented a general learning-based framework for 3-D face landmarking which proposes to characterize, through a statistical model called SFAM, the configurational relationships between the landmarks as well as their local properties in terms of texture and shape. The fitting algorithm locates the landmarks by maximizing the *a posteriori* probability through the optimization of an objective function. The effectiveness of the framework has been demonstrated in the presence of facial expressions and partial occlusions. Consideration of both the global and local properties helps to characterize landmarks deformed under expressions. Furthermore, partial occlusion can be easily taken into account in the objective function provided that the occlusion probability around each landmark can be estimated. Based on this evidence, we have also introduced a 3-D facial occlusion detection and classification algorithm which exhibited a 93.8% classification accuracy on the Bosphorus data set. This detection is based on local shape similarity between local ranges of an input 3-D facial scan and the instances synthesized from the SFAM. The effectiveness of our technique was supported by the experiments on the FRGC data set (v1 and v2), BU-3-DFE containing expressions, and the Bosphorus data set containing partial occlusion.

In this paper, local range and texture maps were used as simple descriptors of local shape and texture around a landmark. In future work, we plan to further improve landmark localization accuracy in considering other descriptors. We also plan to study the generalization capability of the proposed method.

ACKNOWLEDGMENT

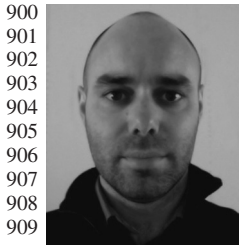
The authors would like to thank the anonymous reviewers for their comments which greatly contributed to the improvement of this paper.

REFERENCES

- 750
- 751 [1] A. A. Salah, H. Cinar, L. Akarun, and B. Sankur, "Robust facial landmarking for registration," *Ann. Telecommun.*, vol. 62, no. 1/2, pp. 1608–1633, 2007.
- 752
- 753
- 754 [2] R. S. Feris, J. Gemmell, K. Toyama, and V. Kruger, "Hierarchical wavelet networks for facial feature localization," in *Proc. 5th IEEE Int. Conf. Autom. Face Gesture Recog.*, Washington, DC, May 20–21, 2002, pp. 125–130.
- 755
- 756
- 757
- 758 [3] F. Y. Shih and C. Chuang, "Automatic extraction of head and face boundaries and facial features," *Inf. Sci.*, vol. 158, pp. 117–130, Jan. 2004.
- 759
- 760 [4] L. Wiskott, J. M. Fellous, N. Kruger, and C. von der Malsburg, "Face recognition by elastic bunch graph matching," *IEEE Trans. Pattern Anal. Mach. Intell.*, vol. 19, no. 7, pp. 775–779, Jul. 1997.
- 761
- 762
- 763 [5] C. Tu and J. J. Lien, "Automatic location of facial feature points and synthesis of facial sketches using direct combined model," *IEEE Trans. Syst., Man, Cybern. B, Cybern.*, vol. 40, no. 4, pp. 1158–1169, Aug. 2010.
- 764
- 765
- 766 [6] K. Bowyer, K. Chang, and P. Flynn, "A survey of approaches and challenges in 3D and multi-modal 3D +2D face recognition," *Comput. Vis. Image Understand.*, vol. 101, no. 1, pp. 1–15, Jan. 2006.
- 767
- 768
- 769 [7] J. D'House, J. Colineau, C. Bichon, and B. Dorizzi, "Precise localization of landmarks on 3D faces using Gabor wavelets," in *Proc. Int. Conf. Biometrics: Theory, Appl., Syst.*, Crystal City, VA, Sep. 27–29, 2007, pp. 1–6.
- 770
- 771
- 772 [8] T. Faltemier, K. Bowyer, and P. Flynn, "Rotated profile signatures for robust 3D feature detection," in *Proc. 8th IEEE Int. Conf. Autom. Face Gesture Recog.*, Amsterdam, The Netherlands, Sep. 17–19, 2008, pp. 1–7.
- 773
- 774
- 775 [9] L. Farkas, *Anthropometry of the Head and Face*, L. G. Farkas, Ed., 2nd ed. New York: Raven, 1994.
- 776
- 777 [10] C. Xu, T. Tan, Y. Wang, and L. Quan, "Combining local features for robust nose location in 3D facial data," *Pattern Recognit. Lett.*, vol. 27, no. 13, pp. 1487–1494, Oct. 2006.
- 778
- 779
- 780 [11] D. Colbry, G. Stockman, and A. Jain, "Detection of anchor points for 3D face verification," in *Proc. IEEE Comput. Soc. Conf. Comput. Vis. Pattern Recog.*, San Diego, CA, Jun. 20–25, 2005, pp. 118–124.
- 781
- 782
- 783 [12] T. F. Cootes, G. Edwards, and C. J. Taylor, "Active appearance models," *IEEE Trans. Pattern Anal. Mach. Intell.*, vol. 23, no. 6, pp. 681–685, Jun. 2001.
- 784
- 785
- 786 [13] T. F. Cootes, C. J. Taylor, D. H. Cooper, and J. Graham, "Active shape models—Their training and application," *Comput. Vis. Image Understand.*, vol. 61, no. 1, pp. 38–59, Jan. 1995.
- 787
- 788
- 789 [14] D. Cristinacce and T. F. Cootes, "Automatic feature localisation with constrained local models," *Pattern Recognit.*, vol. 41, no. 10, pp. 3054–3067, Jan. 2008.
- 790
- 791
- 792 [15] V. Blanz and T. Vetter, "A morphable model for the synthesis of 3D faces," in *Proc. 26th Annu. Conf. Comput. Graph. Interactive Techn.*, Los Angeles, CA, Aug. 8–13, 1999, pp. 187–194.
- 793
- 794
- 795 [16] J. A. Nelder and R. Mead, "A simplex method for function minimization," *Comput. J.*, vol. 7, no. 4, pp. 308–313, Jan. 1965.
- 796
- 797 [17] S. Jahanbin, A. C. Bovik, and H. Choi, "Automated facial feature detection from portrait and range images," in *Proc. IEEE Southwest Symp. Image Anal. Interpretation*, Santa Fe, NM, Mar. 24–26, 2008, pp. 25–28.
- 798
- 799
- 800 [18] Z. Zhang, "Iterative point matching for registration of free-form curves and surfaces," *Int. J. Comput. Vis.*, vol. 13, no. 2, pp. 119–152, Oct. 1994.
- 801
- 802 [19] H. Dibeklioglu, A. A. Salah, and L. Akarun, "3D facial landmarking under expression, pose, and occlusion variations," in *Proc. IEEE Int. Conf. Biometrics: Theory, Appl. Syst.*, Arlington, VA, Sep. 29–Oct. 1, 2008, pp. 1–6.
- 803
- 804
- 805 [20] X. Lu, A. Jain, and D. Colbry, "Matching 2.5D face scans to 3D models," *IEEE Trans. Pattern Anal. Mach. Intell.*, vol. 28, no. 1, pp. 31–43, Jan. 2006.
- 806
- 807
- 808 [21] P. Nair and A. Cavallaro, "3D face detection, landmark localization, and registration using a point distribution model," *IEEE Trans. Multimedia*, vol. 11, no. 4, pp. 611–623, Jun. 2009.
- 809
- 810
- 811 [22] A. Colombo, C. Cusano, and R. Schettini, "3D face detection using curvature analysis," *Pattern Recognit.*, vol. 39, no. 3, pp. 444–455, Mar. 2006.
- 812
- 813 [23] S. Jahanbin, H. Choi, R. Jahanbin, and A. C. Bovik, "Automated facial feature detection and face recognition using Gabor features on range and portrait images," in *Proc. Int. Conf. Image Process.*, San Diego, CA, 2008, pp. 2768–2771.
- 814
- 815
- 816
- 817 [24] V. Bevilacqua, P. Casorio, and G. Mastronardi, "Extending Hough transform to a points cloud for 3D-face nose-tip detection," in *Proc. Int. Conf. Adv. Intell. Comput. Theories Appl.*, Shanghai, China, Sep. 15–18, 2008, pp. 1200–1209.
- 818
- 819
- 820
- 821 [25] Y. Wang, C. Chua, and Y. Ho, "Facial feature detection and face recognition from 2D and 3D images," *Pattern Recognit. Lett.*, vol. 23, no. 10, pp. 1191–1202, Aug. 2002.
- 822
- 823
- 824 [26] B. Gokberk, H. Dutagaci, A. Ulas, L. Akarun, and B. Sankur, "Representation plurality and fusion for 3D face recognition," *IEEE Trans. Syst., Man, Cybern. B, Cybern.*, vol. 38, no. 1, pp. 155–173, Feb. 2008.
- 825
- 826
- 827 [27] C. Boehnen and T. Russ, "A fast multi-modal approach to facial feature detection," in *Proc. IEEE Workshop Appl. Comput. Vis.*, Breckenridge, CO, Jan. 5–7, 2005, pp. 135–142. 829
- 828
- 829
- 830 [28] I. A. Kakadiaris, G. Passalis, G. Toderici, M. Murtuza, Y. Lu, N. Karampatziakis, and T. Theoharis, "Three-dimensional face recognition in the presence of facial expressions: An annotated deformable model approach," *IEEE Trans. Pattern Anal. Mach. Intell.*, vol. 29, no. 4, pp. 640–649, Apr. 2007. 834
- 831
- 832
- 833 [29] M. L. Koudelka, M. W. Koch, and T. D. Russ, "A prescreener for 3D face recognition using radial symmetry and the Hausdorff fraction," in *Proc. Workshop Comput. Vis. Pattern Recog.*, San Diego, CA, Jun. 20–25, 2005, p. 168. 838
- 834
- 835
- 836 [30] X. Lu and A. K. Jain, "Multimodal facial feature extraction for automatic 3D face recognition," Michigan State Univ., East Lansing, MI, Tech. Rep. MSU-CSE-05-22, 2005. 840
- 837
- 838
- 839 [31] P. Szeptycki, M. Ardabilian, and L. Chen, "A coarse-to-fine curvature analysis-based rotation invariant 3D face landmarking," in *Proc. 3rd Int. Conf. Biometrics: Theory, Appl. Syst.*, Washington, DC, 2009, pp. 1–6. 844
- 840
- 841
- 842 [32] X. Lu and A. Jain, "Automatic feature extraction for multiview 3D face recognition," in *Proc. 7th Int. Conf. Autom. Face Gesture Recog.*, Southampton, U.K., Apr. 2–6, 2006, pp. 585–590. 847
- 843
- 844
- 845 [33] Y. Sun and L. Yin, "Facial expression recognition based on 3D dynamic range model sequences," in *Proc. 10th Eur. Conf. Comput. Vis.*, Marseille, France, Oct. 12–18, 2008, pp. 58–71. 850
- 846
- 847
- 848 [34] R. Niese, A. A. Hamadi, F. Aziz, and B. Michaelis, "Robust facial expression recognition based on 3D supported feature extraction and SVM classification," in *Proc. Int. Conf. Autom. Face Gesture Recog.*, Amsterdam, The Netherlands, Sep. 17–19, 2008, pp. 1–7. 854
- 849
- 850
- 851 [35] P. J. Phillips, P. J. Flynn, T. Scruggs, K. W. Bowyer, J. Chang, K. Hoffman, J. Marques, J. Min, and W. Worek, "Overview of the face recognition grand challenge," in *Proc. IEEE Comput. Soc. Conf. Comput. Vis. Pattern Recog.*, San Diego, CA, Jan. 20–25, 2005, vol. 1, pp. 947–954. 858
- 852
- 853
- 854 [36] L. Yin, X. Wei, Y. Sun, J. Wang, and M. Rosato, "A 3D facial expression database for facial behavior research," in *Proc. 7th Int. Conf. Autom. Face Gesture Recog.*, Southampton, U.K., Apr. 10–12, 2006, pp. 211–216. 861
- 855
- 856
- 857 [37] A. Savran, N. Alyuz, H. Dibeklioglu, O. Celiktutan, B. Gokberk, B. Sankur, and L. Akarun, "Bosphorus database for 3D face analysis," in *Proc. 1st COST 2101 Workshop Biometrics Identity Manage.*, 2008, pp. 47–56. 865
- 858
- 859
- 860 [38] P. Soille, *Morphological Image Analysis: Principles and Applications*. New York: Springer-Verlag, 1999. 867
- 861
- 862
- 863 [39] S. Z. Li, *Markov Random Field Modelling in Image Analysis*, 3rd ed. New York: Springer-Verlag, 2009. 869
- 864
- 865
- 866 [40] R. Duda, P. Hart, and D. Stork, *Pattern Classification*. Hoboken, NJ: Wiley, 2001. 870
- 867
- 868
- 869 [41] S. Singer and S. Singer, "Efficient implementation of the Nelder–Mead search algorithm," *Appl. Numer. Anal. Comput. Math.*, vol. 1, no. 2, pp. 524–534, Dec. 2004. 874
- 870
- 871
- 872 [42] P. Perakis, T. Theoharis, G. Passalis, and I. A. Kakadiaris, "Automatic 3D facial region retrieval from multi-pose facial datasets," in *Proc. Eurographics Workshop 3D Object Retrieval*, Munich, Germany, Mar. 30–Apr. 3, 2009, pp. 37–44. 878
- 873
- 874
- 875 [43] P. Perakis, G. Passalis, T. Theoharis, G. Toderici, and I. A. Kakadiaris, "Partial matching of interpose 3D facial data for face recognition," in *Proc. 3rd IEEE Int. Conf. Biometrics: Theory, Appl. Syst.*, Arlington, VA, Sep. 28–30, 2009, pp. 1–8. 882
- 876
- 877
- 878 [44] P. Sinha, B. Balas, Y. Ostrovsky, and R. Russel, "Face recognition by humans: Nineteen results all computer vision researchers should know about," *Proc. IEEE*, vol. 94, no. 11, pp. 1948–1962, Nov. 2006. 885
- 879
- 880
- 881 [45] M. Turk and A. Pentland, "Eigenfaces for recognition," *J. Cogn. Neurosci.*, vol. 3, no. 1, pp. 71–86, Jan. 1991. 887



Xi Zhao (S'XX) received the B.Sc. and M.Sc. degrees (with honors) from the School of Electronic and Information Engineering, Xi'an Jiaotong University, Xi'an, China, in 2003 and 2007, respectively, and the Ph.D. degree (with honors) in computer science from Ecole Centrale Lyon, Ecully, France, in 2010. He is currently conducting research as a Postdoctoral Fellow at the Computational Biomedicine Laboratory, University of Houston, Houston, TX. His research interests include 3-D face analysis, statistical pattern analysis, and computer vision.



Emmanuel Dellandréa received the Master and Engineer degrees in computer science and the Ph.D. degree in computer science from Université de Tours, Tours, France, in 2000 and 2003, respectively.

In 2004, he joined Ecole Centrale Lyon, Ecully, France, as an Associate Professor. His research interests include multimedia analysis, affective computing, and particularly affect recognition both in image and audio signals as well as facial expression analysis.



Liming Chen (M'XX) was awarded the joint B.Sc. degree in mathematics and computer science from the University of Nantes, Nantes, France, in 1984. He obtained the M.S. and Ph.D. degrees in computer science from the University of Paris 6, Paris, France, in 1986 and 1989, respectively.

He first served as an Associate Professor at the Université de Technologie de Compiègne, Compiègne, France, and then joined Ecole Centrale de Lyon, Ecully, France, as Professor in 1998, where he leads an advanced research team on multimedia computing and pattern recognition. From 2001 to 2003, he also served as Chief Scientific Officer in a Paris-based company, Avivias, specialized in media asset management. In 2005, he served as Scientific expert multimedia in France Telecom R&D China. He has been the Head of the Department of Mathematics and Computer Science since 2007. He has taken out three patents, authored more than 100 publications, and acted as Chairman, PC member, and reviewer in a number of high profile journals and conferences since 1995. He has been a (co)-principal investigator on a number of research grants from the European Union FP programme, French research funding bodies, and local government departments. He has directed more than 15 Ph.D. theses. His current research spans from 2-D/3-D face analysis and recognition and image and video analysis and categorization to affect analysis both in image audio and video.



Ioannis A. Kakadiaris (SM'XX) received the B.Sc. degree in physics from the University of Athens, Athens, Greece, the M.Sc. degree in computer science from Northeastern University, Boston, MA, and the Ph.D. degree from the University of Pennsylvania, Philadelphia.

He is a Hugh Roy and Lillie Cranz Cullen Professor of Computer Science, Electrical and Computer Engineering, and Biomedical Engineering at the University of Houston (UH), Houston, TX. He joined UH in August 1997 after a postdoctoral fellowship at the University of Pennsylvania. He is the founder of the Computational Biomedicine Laboratory (www.cbl.uh.edu) and, in 2008, directed the Methodist-University of Houston-Weill Cornell Medical College Institute for Biomedical Imaging Sciences (IBIS) (ibis.uh.edu). His research interests include biometrics, nonverbal human behavior understanding, computational life sciences, energy informatics, computer vision, and pattern recognition.

Dr. Kakadiaris is the recipient of a number of awards, including the National Science Foundation Early Career Development Award, Schlumberger Technical Foundation Award, UH Computer Science Research Excellence Award, UH Enron Teaching Excellence Award, and the James Muller Vulnerable Plaque Young Investigator Prize.

IEEE
PROOF

AUTHOR QUERIES

AUTHOR PLEASE ANSWER ALL QUERIES

Note that your paper will incur overlength page charges of \$175 per page. The page limit for regular papers is 12 pages, and the page limit for correspondence papers is 6 pages.

- AQ1 = The sentence was rephrased for clarity. Please check if the original thought was retained, and correct if necessary.
- AQ2 = “ANR” is defined as “French National Research Agency.” Please check if appropriate, and correct if necessary.
- AQ3 = “ANR-07-MDCO-009-02” and “ANR-07-SESU-004-03” were captured as grants. Please check if appropriate, and correct if necessary.
- AQ4 = “CNRS” was expanded as “Centre National de la Recherche Scientifique.” Please check if appropriate, and correct if necessary.
- AQ5 = “LIRIS” was expanded as “Laboratoire d’InfoRmatique en Image et Systèmes d’information.” Please check if appropriate, and correct if necessary.
- AQ6 = “UMR” was expanded as “Unité Mixte de Recherche.” Please check if appropriate, and correct if necessary.
- AQ7 = “Boehnen *et al.*” was changed to “Boehnen and Russ.” Please check if appropriate, and correct if necessary.
- AQ8 = “Lu *et al.*” was changed to “Lu and Jain.” Please check if appropriate, and correct if necessary.
- AQ9 = “Nair *et al.*” was changed to “Nair and Cavallaro.” Please check if appropriate, and correct if necessary.
- AQ10 = “MAP” is defined as “maximum a posteriori.” Please check if appropriate, and correct if necessary.
- AQ11 = This sentence was rephrased. Please check if the original thought was retained, and correct if necessary.
- AQ12 = All occurrences of “posteriori probability” were changed to “a posteriori probability.” Please check if appropriate, and correct if necessary.
- AQ13 = All occurrences of “kNN” and “K-NN” were captured as “k-NN” to refer to “k-nearest neighbor” and for consistency. Please check if appropriate, and correct if necessary.
- AQ14 = This sentence was rephrased for clarity. Please check if the original thought was retained, and correct if necessary.
- AQ15 = The caption was restructured for clarity of presentation. Please check if appropriate, and correct if necessary.
- AQ16 = The sentence was rephrased for clarity. Please check if the original thought was retained, and correct if necessary.
- AQ17 = Please provide the IEEE membership history of author Xi Zhao.
- AQ18 = The sentence was rephrased. Please check if the original thought was retained, and correct if necessary.
- AQ19 = Please provide the IEEE membership history of author Liming Chen.
- AQ20 = “Master” was changed to “M.S.” Please check if appropriate, and correct if necessary.
- AQ21 = Please validate the address provided for the Université de Technologie de Compiègne.
- AQ22 = Please validate the address provided for Ecole Centrale de Lyon.
- AQ23 = “EU” was expanded as “European Union.” Please check if appropriate, and correct if necessary.
- AQ24 = Please provide the expanded form of “FP.”
- AQ25 = Please provide the IEEE membership history of author Ioannis A. Kakadiaris.
- AQ26 = “NSF” was expanded as “National Science Foundation.” Please check if appropriate, and correct if necessary.

END OF ALL QUERIES

Accurate Landmarking of Three-Dimensional Facial Data in the Presence of Facial Expressions and Occlusions Using a Three-Dimensional Statistical Facial Feature Model

Xi Zhao, *Student Member, IEEE*, Emmanuel Dellandréa, Liming Chen, *Member, IEEE*, and Ioannis A. Kakadiaris, *Senior Member, IEEE*

Abstract—Three-dimensional face landmarking aims at automatically localizing facial landmarks and has a wide range of applications (e.g., face recognition, face tracking, and facial expression analysis). Existing methods assume neutral facial expressions and unoccluded faces. In this paper, we propose a general learning-based framework for reliable landmark localization on 3-D facial data under challenging conditions (i.e., facial expressions and occlusions). Our approach relies on a statistical model, called 3-D statistical facial feature model, which learns both the global variations in configurational relationships between landmarks and the local variations of texture and geometry around each landmark. Based on this model, we further propose an occlusion classifier and a fitting algorithm. Results from experiments on three publicly available 3-D face databases (FRGC, BU-3-DFE, and Bosphorus) demonstrate the effectiveness of our approach, in terms of landmarking accuracy and robustness, in the presence of expressions and occlusions.

Index Terms—Facial expression, fitting, landmarks, occlusion, statistical face model, 3-D face feature.

I. INTRODUCTION

THE RECENT emergence of 3-D facial data has provided an alternative to overcome the challenges in 2-D face recognition, caused by pose changes and lighting variations [6]. Although 2.5D/3-D face data acquisition is known to be insensitive to changes in lighting conditions, the data need to be pose normalized and correctly registered for further face analysis (e.g., 3-D face matching [20], tracking [33], recogni-

tion [26], [28], and facial expression analysis [34]). As most of the existing registration techniques assume the availability of some 2.5D/3-D face landmarks, a reliable localization of these facial feature points is essential.

A. Related Work

Although there is no general consensus yet, we consider stable facial landmarks to be the fiducial points defined by anthropometry [9] that have consistent reproducibility even in adverse conditions such as facial expression or occlusion. Stable facial landmarks generally include the nose tip, the inner eye corners, the outer eye corners, and the mouth corners. Such landmarks are not only characterized by their own properties, in terms of local texture and local shape, but are also characterized by their global structure resulting from the morphology of the face. Therefore, local feature information and the configurational relationships of landmarks are jointly important for accurate and robust face landmarking. This finding is coherent with human studies on face analysis suggesting that both local features and configurational relationships are important [44].

Despite the increasing amount of related literature, 3-D face landmarking is still an open problem. Current face landmarking techniques lack both accuracy and robustness, particularly in the presence of lighting variations, head pose variations, scale changes, facial expressions, self-occlusions, and occlusion by accessories (e.g., hair, moustache, and eyeglasses) [1]. This paper proposes a data-driven general framework for precise 3-D face landmarking, which is robust to changes in facial expressions and partial occlusions.

Face landmarking on 2-D facial texture images has been extensively studied [1], and several approaches have been proposed. These approaches can be classified into appearance-based [2], geometry-based [3], and structure-based approaches [4], [5]. Interesting approaches include 2-D statistical models, such as the popular active appearance model [12] or the more recent constrained local model (CLM) [14], which perform statistical analysis both on the facial appearance and the 2-D shape. However, since they are applied to 2-D texture images, these approaches inherit the sensitivity to lighting and pose changes.

Manuscript received December 23, 2009; revised November 18, 2010, February 14, 2011, and March 29, 2011; accepted April 8, 2011. This work was supported in part by the French National Research Agency (ANR) through the ANR Omnia project under Grant ANR-07-MDCO-009-02 and through the ANR FAR 3-D project under Grant ANR-07-SESU-004-03. This paper was recommended by Associate Editor J. Su.

X. Zhao and I. A. Kakadiaris are with the Computational Biomedicine Laboratory, Department of Computer Science, University of Houston, Houston, TX 77204-3010 USA (e-mail: zhaoxi@ieee.org; ioannisk@uh.edu).

E. Dellandréa and L. Chen are with the Université de Lyon, Centre National de la Recherche Scientifique, Ecole Centrale Lyon, Laboratoire d'InfoRmatique en Image et Systèmes d'information, Unité Mixte de Recherche 5205, 69134 Ecully Cedex, France (e-mail: emmanuel.dellandrea@ec-lyon.fr; liming.chen@ec-lyon.fr).

Color versions of one or more of the figures in this paper are available online at <http://ieeexplore.ieee.org>.

Digital Object Identifier 10.1109/TSMCB.2011.2148711

74 Research on 3-D face landmarking is rather recent. Most of
 75 the existing methods embed *a priori* knowledge on landmarks
 76 on 3-D face by computing the response to local 3-D shape-
 77 related features (e.g., spin image [28], [42], [43], effective
 78 energy [10], Gabor filtering [7], [11], generalized Hough trans-
 79 form [24], local gradients [19], HK curvature [22], shape index
 80 [20], [42], [43], curviness index [21], and radial symmetry
 81 [29]). While these approaches enable a rather accurate detection
 82 of landmarks that are shape prominent (e.g., the nose tip or the
 83 inner corners of eyes), their localization accuracy drastically
 84 decreases for other less prominent landmarks.

85 As current 3-D imaging systems can deliver registered range
 86 and texture images, a straightforward method to discriminate a
 87 landmark is to accumulate evidence from both face representa-
 88 tions (i.e., face geometry and texture). Boehnen and Russ [27]
 89 computed the eye and mouth maps based on both color and
 90 range information. Wang *et al.* [25] used a “point signature”
 91 representation to code a 3-D face mesh as well as Gabor
 92 jets of landmarks from the 2-D texture image. Gabor wavelet
 93 coefficients [1], [23] were used to model the local appearance
 94 in the texture map and local shape in a range map around
 95 each landmark. Lu and Jain [32] proposed to compute and fuse
 96 the shape index response (range) and the cornerness response
 97 (texture) in local regions around seven feature points.

98 As the combinations of candidate landmarks resulting from
 99 shape and/or texture related descriptors are generally impor-
 100 tant, some studies also proposed to make use of the structure
 101 between landmarks. This is accomplished by using heuristics
 102 [21], a 3-D geometry-based confidence [27], an extended elastic
 103 bunch graph [23], or a simple mean model constructed as the
 104 average 3-D position of landmarks from a learning data set
 105 [30]. However, there is no technique that best takes into account
 106 both the configurational relationships between landmarks and
 107 the local properties in terms of geometric shape/texture around
 108 each landmark.

109 Furthermore, only few of the aforementioned studies address
 110 the issue of face landmarking in the presence of facial expres-
 111 sions or occlusions. Nair and Cavallaro [21] used their 3-D
 112 point distribution model (PDM) to locate five landmarks (the
 113 two outer eye points, the two inner eye points, and the nose
 114 tip) under facial expressions with a locating accuracy ranging
 115 from 8.83 mm for the nose tip to 20.46 mm for the right outer
 116 eye point. However, all the five landmarks were located on
 117 stable face regions during facial expressions. Dibeklioglu *et al.*
 118 [19] studied 3-D facial landmarking under expression, pose,
 119 and occlusion variations. They built statistical models of local
 120 features around landmark locations using a mixture of factor
 121 analysis in order to determine landmark locations on a coarse
 122 level. Heuristics were then applied to locate the nose tip at a
 123 fine level. Using the configurational relationships and geometry
 124 features, Perakis *et al.* [42], [43] addressed landmarking on
 125 3-D facial data under multiple orientations, taking into account
 126 missing data due to self occlusion.

127 B. Proposed Approach

128 In this paper, we propose a general learning-based framework
 129 for 3-D face landmarking which combines both configurational

relationships between the landmarks and their local properties 130
 in a principled way, through optimization of a global objective 131
 function. This data-driven based approach aims to overcome 132
 the shortcomings of the previous feature-based approaches that 133
 require the embedding of a discriminative prior knowledge for 134
 each landmark. Instead, it relies on a statistical model, called 135
 3-D Statistical Facial feAture Model (SFAM), which learns 136
 both the global variations in 3-D face morphology and the local 137
 variations around each 3-D face landmark in terms of texture 138
 and geometry. To train the model, we manually labeled the tar- 139
 get landmarks for each aligned frontal 3-D face. Preprocessing 140
 is first performed to enhance the quality of facial scans, and 141
 then, the scans are remeshed to normalize the face scale. The 142
 SFAM is then constructed by applying principle component 143
 analysis (PCA) to the global 3-D face landmark configurations, 144
 the local texture, and the local shape around each landmark 145
 from the training facial data. PCA-based learning is popular 146
 for face recognition since human faces are similar, and hence, 147
 it is quite reasonable to assume that the properties of facial 148
 features follow a Gaussian distribution, as demonstrated by 149
 previous studies (e.g., eigenfaces [45]). In our approach, only 150
 the salient variation modes (95% of the variation) for the 151
 three representations (morphology, texture, and geometry) are 152
 retained. By varying the control parameters of SFAM, different 153
 3-D partial face instances that consist of local face regions with 154
 texture and shape (structured by their global 3-D morphology) 155
 can be generated. In this paper, we have used a simple local 156
 range map and an intensity map to characterize the local shape 157
 and texture properties around each landmark. Alternatively, the 158
 SFAM may use all the aforementioned descriptors of local 159
 features around each landmark (e.g., mean and Gaussian curva- 160
 ture or shape index for local shape characterization and Gabor 161
 jets or cornerness response for local texture description). An 162
 interesting property for the characterization of the local shape 163
 around a landmark is that the descriptor is sufficiently robust 164
 against shape deformation, which typically occurs in facial 165
 expressions. Popular geometric descriptors (e.g., shape index or 166
 HK curvatures) provide an accurate local shape description and 167
 are sensitive to geometric shape differences. However, when the 168
 normalized correlation is used as the similarity measure, local 169
 shape properties described by raw range maps are less discrim- 170
 inative with respect to identity and deformations. Similarly, the 171
 description of local texture should be tolerant to changes caused 172
 by lighting or expressions. A similar reasoning also applies to 173
 using the raw texture maps for texture characterization. The 174
 combination of raw texture maps and the similarity measure 175
 relieves, to some extent, the effect of lighting conditions and 176
 expressions on texture. Our experiments indicate that the use 177
 of a local raw range map and a local raw texture map around 178
 each landmark provides a good tradeoff between computational 179
 efficiency and robustness. Although a comprehensive study of 180
 the selection of robust local features is needed, it is beyond the 181
 scope of this paper. 182

Our learning-based framework can be considered as a natural 183
 extension of the morphable 3-D face model [15] and the CLM 184
 [14] as we propose to learn, at the same time, the global vari- 185
 ations of 3-D face morphology and the local ones in terms of 186
 texture and shape around each landmark. Fitting the SFAM on 187

TABLE I
SUMMARY OF SYMBOLS

Symbols	Description
s	3D facial landmark configuration vector
g	Intensity vector
z	Geometry vector
ψ	SFAM
P	Learnt modes of variations
b	SFAM parameters
T	Texture map of a 3D facial scan
R	Range map of a 3D facial scan
m	Occlusion mask

188 a probe facial scan is accomplished by maximum *a posteriori*
 189 (MAP) probability. The fitted morphology instance delivers
 190 the locations of targeted landmarks. Using 3-D training faces
 191 with expressions, the SFAM has the ability to learn expression
 192 variations and generate instances with the learned variations
 193 so as to increase the *a posteriori* probability in fitting faces
 194 with expression. Furthermore, we propose to use a *k*-nearest
 195 neighbor (*k*-NN) classifier to identify the partially occluded
 196 faces and the type of occlusion. A histogram of the similarity
 197 map between the local shapes of the target face and shape
 198 instances from the SFAM is used as the input. This information
 199 about occlusions is also integrated into the objective function
 200 used in the fitting process to handle landmarking on partially
 201 occluded 3-D facial scans.

202 The main contributions of this paper are the following.

- 203 1) We build an SFAM that elegantly combines the global and
 204 local features extracted from three facial representations.
- 205 2) An occlusion detection and classification algorithm is
 206 proposed to detect occlusions and classify them into
 207 different types, thereby providing occlusion information
 208 to the fitting algorithm.
- 209 3) A fitting algorithm is proposed to locate landmarks
 210 through optimizing an objective function, implemented
 211 on local patch-based correlation meshes. In addition, the
 212 fitting algorithm incorporates occlusion knowledge and
 213 thus is able to locate landmarks on partially occluded
 214 faces.

215 The rest of this paper is organized as follows. In Section II,
 216 our statistical model SFAM is introduced. In Section III, the
 217 objective function that combines the local shape and texture
 218 properties and the fitting algorithm are described. Section IV
 219 addresses 3-D face partial occlusion. Experimental results are
 220 discussed in Section V, while Section VI concludes this paper.
 221 Table I presents a summary of the different symbols used in this
 222 paper.

223 II. SFAM

224 Three-dimensional facial data acquired by the current 3-D
 225 imaging systems are usually noisy and may contain holes and
 226 spikes. Hence, we first preprocess all the 3-D facial scans to
 227 remove noise. Head pose and scale variations are normalized by
 228 alignment and remeshing (see Section II-A). Then, we model
 229 the variations in 3-D configurations of landmarks and their
 230 local variations in terms of texture and shape around each
 231 landmark (see Section II-B). New partial 3-D face instances can
 232 be synthesized from the learned model (see Section II-C).

A. Preprocessing the Training Facial Data

233

To remove the noise (e.g., spikes and holes) and enhance
 the quality of 3-D facial scans, we perform the following
 operations.

- 1) Median cut: Spikes are detected by checking the discon-
 tinuity of points and are removed by the application of a
 median filter.
- 2) Hole filling: Holes that are caused by the 3-D scanner
 and the removed spikes are located on the range maps of
 facial scans by a morphological reconstruction [38] and
 filled by cubic interpolation. The open mouth is excluded
 from this preprocessing step by estimating the size of
 the hole corresponding to the open mouth region with an
 empirically set threshold.

Although faces are usually scanned from a frontal viewpoint,
 variations in head pose still exist and interfere with the learning
 of global variations in 3-D facial morphology. Consequently,
 these variations may perturb the learning of local shape and
 texture variations. To compensate for head pose variations,
 the facial data are first translated close to the origin of the
 coordinate system. The iterative closest point algorithm [18]
 is then used to minimize the difference between the two
 point clouds of the new scan and the selected facial scan,
 which holds a frontal and straight pose. Since the head pose
 variations have been compensated after alignment, the SFAM
 can be learned with more accurate variations in local face
 texture and geometry.

To train the model, the targeted anthropometric landmarks
 have to be manually labeled for each aligned frontal 3-D face.
 This is the major difference between the proposed approach
 and most of the existing 3-D face landmarking algorithms.
 Instead of directly embedding *a priori* knowledge on landmarks
 into the landmarking algorithm, we propose a data-driven
 approach which, through statistical learning, encodes into a
 model discriminatory information of targeted landmarks, in
 terms of their global configurational relationships as well as
 the properties of local texture and shape around each landmark.
 For any given training data set, the set of targeted landmarks
 can be easily changed according to the particular application.
 This general characteristic of the proposed approach is
 demonstrated in our experiments on three different public
 data sets: FRGC, BU-3-DFE, and Bosphorus data sets. Most
 landmarks out of 15 (as illustrated in Fig. 5) on the FRGC
 data set were selected from the rigid part of the face as they
 were subsequently used for 3-D face recognition. On the other
 hand, landmarks on the BU-3-DFE and the Bosphorus data sets
 (as illustrated in Figs. 6 and 8) encompass anthropometric
 points from all facial regions as they are used for facial
 expression analysis.

To learn the local geometry and texture around each
 landmark, it is necessary to have the same number of points
 in a local region and have a dense correspondence among
 different faces. However, changes due to face scale and
 subject identity make this normalization difficult. Therefore,
 we use uniform grids to remesh local regions around
 landmarks. First, all the points are sampled from point
 clouds within a specified distance from each landmark.
 The number of sampled points, or the point density, in
 local regions varies from face to face due

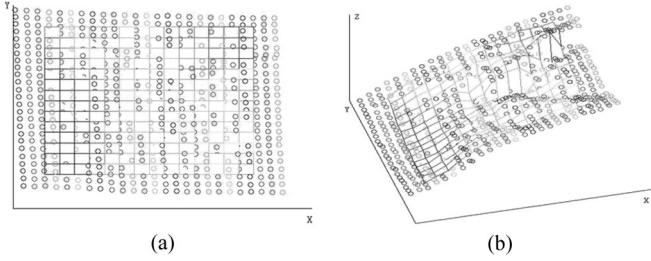


Fig. 1. Scale normalization in a local region associated to the left corner of the left eye from the (a) frontal view and (b) side view. Circles denote sampled points from the 3-D face model, and the grid is composed of the interpolated points. Interpolation is also performed on the point intensity values.

290 to face scale. Second, a uniform grid is associated with each
291 landmark. As illustrated in Fig. 1, each grid is centered at its
292 corresponding landmark with a size of 15×15 (225 nodes on a
293 grid) and a resolution of 1 mm (the intervals of grids on the X ,
294 Y dimensions are fixed to 1 mm). The z values of a node (and
295 the associated intensity values) on a grid are interpolated from
296 the range values of sampled points. Using this normalization, a
297 fixed number of points can be obtained regardless of face scale
298 and subject identity. Thus, the point-to-point correspondence
299 among faces is established easily and efficiently.

300 B. Modeling the Configurational Relationships and Local 301 Shape and Texture Features of the Landmarks

302 Once a 3-D facial scan is preprocessed, 3-D coordinates of all
303 the landmarks (3-D morphology) are concatenated into a vector
304 \mathbf{s}_i , which describes the configurational relationships among
305 local regions

$$\mathbf{s}_k = (x_1, y_1, z_1, x_2, y_2, z_2, \dots, x_N, y_N, z_N)^T \quad (1)$$

306 where N is the number of landmarks (e.g., in this paper, $N =$
307 15 or 19).

308 We further generate the two vectors \mathbf{g}_k and \mathbf{z}_k by concate-
309 nating intensity and range values on all the grids on a face
310 (M is the number of interpolated points collected from all the
311 local regions). The \mathbf{z}_k vectors capture the variations of local
312 geometric shapes around each landmark while the \mathbf{g}_k vectors
313 capture the local texture properties

$$\mathbf{g}_k = (g_1^k, g_2^k, \dots, g_M^k)^T, \quad \mathbf{z}_k = (z_1^k, z_2^k, \dots, z_M^k)^T. \quad (2)$$

314 PCA is then applied to the three vector sets $\{\mathbf{s}_k\}$, $\{\mathbf{g}_k\}$, and
315 $\{\mathbf{z}_k\}$, extracted from the training 3-D facial data (k denotes
316 the k th training example). Thus, three linear models are built
317 by retaining 95% of the variance in landmark configurations as
318 well as local texture and shape around each landmark. The three
319 models are represented as follows:

$$\mathbf{s} = \bar{\mathbf{s}} + \mathbf{P}_s \mathbf{b}_s \quad (3)$$

$$\mathbf{g} = \bar{\mathbf{g}} + \mathbf{P}_g \mathbf{b}_g, \quad \mathbf{z} = \bar{\mathbf{z}} + \mathbf{P}_z \mathbf{b}_z \quad (4)$$

320 where $\bar{\mathbf{s}}$, $\bar{\mathbf{g}}$, and $\bar{\mathbf{z}}$ are the mean landmark configuration, the
321 mean intensity, and the mean range value, respectively, while

\mathbf{P}_s , \mathbf{P}_g , and \mathbf{P}_z are the three sets of modes of configuration, 322
intensity, and depth variation, respectively. The terms \mathbf{b}_s , \mathbf{b}_g , 323
and \mathbf{b}_z are the corresponding sets of control parameters. All 324
individual components in \mathbf{b}_s , \mathbf{b}_g , and \mathbf{b}_z are independent. 325
We further assume that all the \mathbf{b}_q -parameters, where $\mathbf{b}_q \in$ 326
($\mathbf{b}_s, \mathbf{b}_g, \mathbf{b}_z$), follow a Gaussian distribution with zero mean and 327
standard deviation σ_q . 328

C. Synthesizing Instances From a New Face

329 Given the parameters \mathbf{b}_s , a configuration instance can be 330
generated using (3). Then, given a new facial scan, the set of 331
scan points closest to the configuration instance is computed. 332
Based on these points, the vectors \mathbf{g}^n and \mathbf{z}^n are obtained by 333
applying the process described in the training phase (2). Then, 334
 \mathbf{b}_g and \mathbf{b}_z are estimated as follows: 335

$$\mathbf{b}_g = \mathbf{P}_g^T (\mathbf{g}^n - \bar{\mathbf{g}}), \quad \mathbf{b}_z = \mathbf{P}_z^T (\mathbf{z}^n - \bar{\mathbf{z}}). \quad (5)$$

\mathbf{b}_g and \mathbf{b}_z are limited to the range $[-3\sigma, 3\sigma]$. Then, using 336
these constrained \mathbf{b}_g and \mathbf{b}_z , we can generate texture and shape 337
instances $\hat{\mathbf{g}}^n$ and $\hat{\mathbf{z}}^n$ by using (4). The landmarks, along with 338
their local texture and local shape instances, compose a partial 339
face instance. 340

III. LOCALIZING LANDMARKS

341 The SFAM-based landmark localization procedure consists 342
of MAP probability of landmark configuration, given a 3-D 343
facial scan to be landmarked, and leads to optimizing an 344
objective function. In Section III-A, we present the objective 345
function to be optimized, and in Section III-B, we introduce the 346
fitting algorithm for localizing landmarks. We then discuss our 347
assumptions in Section III-C. 348

A. Objective Function and MAP

349 We first define the objective function $f(\mathbf{b}_s) = p(\mathbf{s}|T, R, \psi)$ 350
as the *a posteriori* probability of landmark configuration \mathbf{s} to be 351
maximized for a 3-D facial scan represented by its texture map 352
 T and range map R and the learned statistical model SFAM ψ . 353
Using the Bayes rule, we obtain 354

$$\begin{aligned} p(\mathbf{s}|T, R, \psi) &= p(T, R, \mathbf{s}, \psi) / p(T, R, \psi) \\ &\propto p(T, R|\mathbf{s}, \psi) p(\mathbf{s}|\psi) \\ &\propto p(T|\mathbf{s}, \psi) p(R|\mathbf{s}, \psi) p(\mathbf{s}|\psi) \end{aligned} \quad (6)$$

where $p(T|\mathbf{s}, \psi)$ and $p(R|\mathbf{s}, \psi)$ are the probabilities of having 355
the facial texture T and the range R , given a landmark configu- 356
ration \mathbf{s} and SFAM ψ , respectively. We assume that the random 357
variables R and T from the different facial representations 358
are independent within a local face region. The term $p(\mathbf{s}|\psi)$ 359
denotes the probability of having a landmark configuration \mathbf{s} 360
given the SFAM ψ . Thus, the prior $p(\mathbf{s}|\psi)$ can be estimated 361
using the assumption of Gaussian distribution on the corre- 362
sponding control parameters \mathbf{b}_j in the third term of (7). 363

364 The probabilities $p(T|s, \psi)$ and $p(R|s, \psi)$ can be estimated
 365 using the Gibbs–Boltzmann distribution as described in

$$p(s|T, R, \psi) \propto \prod_{i=1}^N e^{-(\alpha\eta_i)} \prod_{i=1}^N e^{-(\beta\gamma_i)} \prod_{j=1}^K e^{-\frac{b_j^2}{\lambda_j}}$$

$$\log p(s|T, R, \psi) \propto \sum_{i=1}^N (-\alpha\eta_i) + \sum_{i=1}^N (-\beta\gamma_i) - \sum_{j=1}^K \frac{b_j^2}{\lambda_j} \quad (7)$$

366 where N is the number of local regions, η_i and γ_i are the energy
 367 functions of the associated local region i in terms of texture and
 368 range properties, respectively, given the landmark configuration
 369 s and the SFAM ψ , and α and β are weight constants. The
 370 third term in (7) represents the Mahalanobis distance [13],
 371 where K is the number of retained landmark configuration
 372 modes and λ_j denotes the corresponding eigenvalue in the
 373 landmark configuration model. b_j denotes the control parameter
 374 that generates the landmark configuration s given the statistical
 375 model ψ . For the energy functions η_i and γ_i , high energies
 376 occur when the corresponding local texture T_i and range R_i do
 377 not match the texture and range instances which are generated
 378 by the SFAM ψ given the landmark configuration s . In this
 379 paper, instead of using the distances in these energy functions
 380 to express the degree of mismatch, we use a similarity measure,
 381 namely, the normalized correlations defined in (9), and derive
 382 the following objective function $f(\mathbf{b}_s)$ (thereby changing the
 383 polarity of the terms associated with η_i and γ_i):

$$f(\mathbf{b}_s) = \alpha \sum_{i=1}^N m_i F_{gi}(s_i) + \beta \sum_{i=1}^N m_i F_{zi}(s_i) - \sum_{j=1}^k \frac{b_j^2}{\lambda_j} \quad (8)$$

384 where F_{gi} and F_{zi} are explained in (9) and m_i is introduced
 385 to address partially occluded facial data. The term m_i is the
 386 probability of the region around the i th landmark being un-
 387 occluded. The term s_i denotes the landmark location from the
 388 morphology model. Specifically

$$F_{gi} = \left\langle \frac{\mathbf{g}_i}{\|\mathbf{g}_i\|}, \frac{\hat{\mathbf{g}}_i}{\|\hat{\mathbf{g}}_i\|} \right\rangle \quad F_{zi} = \left\langle \frac{\mathbf{z}_i}{\|\mathbf{z}_i\|}, \frac{\hat{\mathbf{z}}_i}{\|\hat{\mathbf{z}}_i\|} \right\rangle \quad (9)$$

389 where $\langle \cdot, \cdot \rangle$ is the inner product and $\|\cdot\|$ is the L_2 norm. The
 390 values of α and β are fixed and are computed as the ratios
 391 of $\sum_{i=1}^N F_{gi}$ and $\sum_{j=1}^K (b_j^2/\lambda_j)$, $\sum_{i=1}^N F_{zi}$, and $\sum_{j=1}^K (b_j^2/\lambda_j)$,
 392 respectively, during the offline training.

393 In this paper, we have used a simple occlusion classification
 394 algorithm which delivers a binary value for m_i : zero if the local
 395 region is occluded and one if the region is not occluded.

396 B. Fitting Algorithm

397 Landmarking a 3-D facial scan consists of fitting the SFAM
 398 ψ while maximizing the objective function (8). First, the 3-
 399 D facial scan is preprocessed as described in Section II-A,
 400 including spike removal, hole filling, and head pose normal-
 401 ization. The occlusion algorithm, introduced in Section IV, is
 402 then applied to identify the occluded local regions and then
 403 used to set the corresponding m_i coefficients to zero. Therefore,
 404 only the unoccluded local regions are considered in the fitting
 405 process. The algorithm works in a straightforward manner and
 406 is described in Algorithm 1.

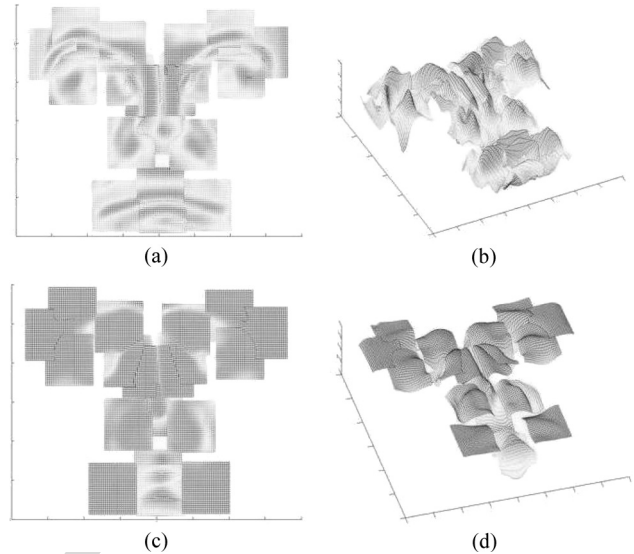


Fig. 2. Depiction of the correlation meshes from the frontal and side views. These meshes capture the similarity between instances and local facial regions in both texture and shape representations. The red color corresponds to large correlation values while blue corresponds to small correlation values. Large values on the correlation meshes correspond to large probabilities of finding landmarks on their locations. The meshes are in four-dimensional space, where the first three dimensions are x , y , z and the last dimension represents correlation values. In these figures, we display the correlation values instead of z . (a,b) Two viewpoints of the same correlation mesh capturing the similarity of texture (intensity) instances from SFAM and local texture regions (intensity) on a given face. (c,d) Correlation mesh capturing the similarity of shape (range) instances from SFAM and the local face shapes (range).

Algorithm 1 SFAM Fitting

Input: A 3-D scan and a trained SFAM.

1. Optimize the morphology parameters \mathbf{b}_s to minimize the distance between corresponding morphology instances and their closest points on the input facial data, and obtain a set of points \mathcal{S} .
 2. Synthesize texture and shape instances \hat{G} , \hat{Z} as described in Section II-C using \mathcal{S} .
 3. Normalize local regions around points \mathcal{S} within a neighborhood large enough to cover the potential landmark locations as in Section II-A, creating a set of local mesh \mathcal{G} , \mathcal{Z} .
 4. Compute correlation meshes on both texture and geometry representations (see Fig. 2) by correlating \hat{G} , \hat{Z} with G , Z , respectively, which are different parts of \mathcal{G} , \mathcal{Z} sampled by a sliding window (size of 15×15) on local regions (9).
 5. Optimize the morphology parameters \mathbf{b}_s to reach the maximum of the sum of values on the two correlation meshes while minimizing the Mahalanobis distance associated with the landmark configuration defined by the control parameters \mathbf{b}_s .
- Output:** Optimized morphology parameters \mathbf{b}_s .

The optimization process in steps one and five of the algorithm is processed by the Nelder–Mead simplex algorithm [16]. Once convergence is reached, the instance s resulting from the optimized \mathbf{b}_s indicates the location of landmarks. For partially occluded faces, occluded landmarks and their corresponding local meshes are excluded from the optimization process. In the case of incorrect occlusion classification, local nonface meshes lead the optimization to converge to an unpredictable point far from the desired minimum.

436 C. Discussion

437 To deduce (7), we assumed that the probabilities $p(T|s, \psi)$
 438 and $p(R|s, \psi)$ follow a Gibbs–Boltzmann distribution. This
 439 assumption is reasonable and motivated by the fact that the
 440 problem of 3-D face landmarking is actually a Markov random
 441 field (MRF) which consists of assigning a label from a set of
 442 labels \mathcal{L} to each vertex of a 3-D facial scan. The set \mathcal{L} encom-
 443 passes all targeted landmarks (e.g., nose tip and eye corners)
 444 and a null value labeling any vertex which is not the location
 445 of a targeted landmark. Then, the theorem of the equivalence
 446 between MRFs and Gibbs distributions defined by Hammersley
 447 and Clifford [39] implies that the probabilities $p(T|s, \psi)$ and
 448 $p(R|s, \psi)$ follow a Gibbs–Boltzmann distribution [40].

449 We also used the Nelder–Mead simplex algorithm [16],
 450 which is one of the best known algorithms for multidimensional
 451 unconstrained optimization without derivatives. This method
 452 does not require any derivative information and is widely used
 453 to solve parameter estimation and statistical problems of similar
 454 nature [41].

455 IV. OCCLUSION DETECTION AND CLASSIFICATION

456 Facial data analysis in the presence of partial occlusions
 457 (caused by a variety of factors such as hair, glasses, mustaches,
 458 and scarf) is a difficult problem. In 3-D facial landmarking, only
 459 occlusions which may occur in local regions around landmarks
 460 are of interest. Thus, in this paper, we adopt an approach to
 461 classify the occlusion type and provide a set of binary values to
 462 local regions: either occluded or not occluded. Alternatively, we
 463 may compute a probability associated with a local region being
 464 occluded or a measure indicating roughly the extent to which a
 465 local region is occluded.

466 To perform occlusion detection, features from the range map
 467 are extracted as the presence of occlusion definitively changes
 468 local shape. Therefore, given a new facial scan, its closest points
 469 to the mean landmark configuration $\bar{s}(3)$ are first computed.
 470 Then, grids (50×50) are used to remesh local regions around
 471 these points for range values (see Section II-A). The size of
 472 local regions is chosen to be large enough to account for
 473 variations due to scale and subject changes as well as to cover
 474 the local regions near landmarks for occlusion detection.

475 For each local region i , processing is performed in a sliding
 476 window manner (the size of the sliding window is the same as
 477 the size of the local regions considered in the SFAM). At each
 478 step, we compute a local depth map Z_α and its local shape
 479 instance Z_β to further obtain a similarity L_S as follows:

$$b_{alpha} = P_{z,i}^T(Z_\alpha - \bar{z}_i), Z_\beta = \bar{z}_i + P_{z,i}b_\beta \quad (10)$$

$$L_S = \left\langle \frac{Z_\alpha}{\|Z_\alpha\|}, \frac{Z_\beta}{\|Z_\beta\|} \right\rangle \quad (11)$$

480 where $P_{z,i}$ is the submatrix composed of the rows in P_z
 481 associated with local region i . The term \bar{z}_i is the subvector
 482 composed of the rows in \bar{z} also associated with local region i .
 483 The term b_β is obtained by limiting b_α within the boundary as
 484 described in Section II-C. In the case of occlusion, b_α does not
 485 necessarily obey a Gaussian distribution and may be distributed

far away from the mean value. Thus, by boundary limitation, the
 instances Z_β are different from the occluded local shape Z_α ,
 leading to a low similarity value in (11).

The local similarity value L_S is computed for all points in
 a local region, leading to a local similarity map. We then build
 a histogram of L_S values using 50 bins to represent the values
 ranging from -1 to 1 . Since most values in the local similarity
 map are close to 1 , we allocate more bins near 1 . Then, the his-
 tograms computed from all the local regions are concatenated
 into a single feature vector. Partially occluded 3-D facial scans
 in the training set are manually labeled according to a given
 occlusion type (i.e., occlusion in the ocular region, occlusion
 in the mouth region, occlusion by glasses, or unoccluded). The
 distance between histograms is computed using the Euclidean
 metric, and the classification is performed using a simple k -NN
 classifier.

In our experiments, we used the Bosphorus data set which
 encompasses partially occluded 3-D facial scans according to
 several occlusion patterns. We preset a set of binary values
 indicating the occlusion state in each local region for each
 occlusion pattern. By classifying facial scans into these states,
 we can thus obtain a list of local regions that are occluded
 $[m_i$ in (8)].

V. EXPERIMENTAL RESULTS

The proposed statistical learning-based framework for 3-D
 facial landmarking was applied on three data sets, namely, the
 FRGC [35], BU-3-DFE [36], and Bosphorus [37] data sets. In
 Section V-A, we describe the data sets and the experimental
 setup and present the various experimental results in the follow-
 ing sections. These results are further discussed in Section V-E.

A. Data Sets and Experimental Setup

The FRGC data set includes two versions. FRGC v1 con-
 tains 953 scans from 275 people, captured under controlled
 illumination conditions and generally neutral expressions [35].
 However, these 953 facial scans have slight head pose and scale
 variation. In addition, FRGC v1 contains 33 noisy 3-D facial
 scans having uncorrected correspondence between the range
 and texture maps. These scans were not used in our experi-
 ment. FRGC v2 contains 4007 facial scans from 466 persons.
 These 3-D facial scans were captured under different illumina-
 tion conditions and contain various facial expressions (such as
 happiness or surprise).

The BU-3-DFE database contains data from 100 subjects
 [36]. Each subject performed a neutral expression and six uni-
 versal expressions in front of a 3-D scanner. Each of these six
 universal expressions (happiness, disgust, fear, anger, surprise,
 and sadness) is displayed with four levels of intensity. In our
 experiments, we have used the neutral facial data and facial data
 with expressions in the two high-level intensities from all the
 subjects, resulting in 1300 facial scans in total.

The Bosphorus data set contains 3396 facial scans from 104
 subjects [37]. This data set contains not only the six universal
 facial expressions but also 3-D scans under realistic occlusions
 (e.g., glasses, hands around the mouth, and eye rubbing).

TABLE II
CONFUSION MATRIX OF OCCLUSION CLASSIFICATION

	Eye	Mouth	Glass	Unoccluded
Eye	93.3 %	2.2 %	2.4 %	2.1 %
Mouth	1.0 %	97.4 %	1.6 %	0.0 %
Glass	7.3 %	3.3 %	84.4 %	4.5 %
Unoccluded	0.0 %	0.0 %	0.0 %	100.0 %

540 Moreover, the data set includes many male subjects that have
541 moustache and beard.

542 As illustrated in Figs. 5–8, we manually labeled 15 facial
543 landmarks in the FRGC data set and used 19 labeled landmarks
544 in the BU-3-DFE and Bosphorus data sets. They were used
545 as ground truth for learning the SFAM model and testing our
546 landmark fitting algorithm. These three landmark data sets
547 contain some common landmarks, such as eye corners and
548 mouth corners, which are sensitive to facial expressions.

549 B. Occlusion Classification Results

550 The proposed algorithm for occlusion detection was applied
551 to 3-D scans from the Bosphorus data set. In our experiment,
552 we excluded partial occlusions by hair as they do not occur in
553 the landmark regions. We have considered partial occlusions
554 caused by glasses, a hand near the mouth region, and a hand
555 near the ocular region in addition to unoccluded 3-D scans.
556 We experimentally set k to five in the k -NN classifier and
557 performed a two-fold cross-validation. The confusion matrix
558 is provided in Table II. An average classification accuracy up
559 to 93.8% is achieved, which appears to be sufficient for the
560 subsequent landmarking task.

561 C. Results on SFAM

562 We used 452 scans from the FRGC v1 data set to build
563 the SFAM-1 model by learning the local properties around
564 15 landmarks and their configurational relationships. The train-
565 ing facial scans have limited illumination variations and do not
566 contain facial expressions.

567 Furthermore, we used facial scans from 11 subjects in the
568 BU-3-DFE data set and the first 32 subjects in the Bosphorus
569 data set to build the SFAM-2 and SFAM-3, respectively. For
570 every subject, 13 scans were used for training in the case of
571 the BU-3-DFE data set (a neutral scan and the two scans for
572 each of the six universal expressions at the intensity levels three
573 and four), and seven scans in the case of the Bosphorus data
574 set (a neutral scan and a scan for each of the six universal
575 expressions). Fig. 3 illustrates the SFAM-3 learned from the
576 Bosphorus data set containing the first mode of configuration,
577 local texture, and local shape for variances $3 \pm \sigma$.

578 D. Results on Landmarking

579 Using the learned statistical models, the fitting algorithm
580 for 3-D face landmarking was evaluated on three different
581 experimental setups. In all these experiments, the errors were
582 computed as the Euclidean distance between the automatically
583 localized and the corresponding manually labeled landmarks.

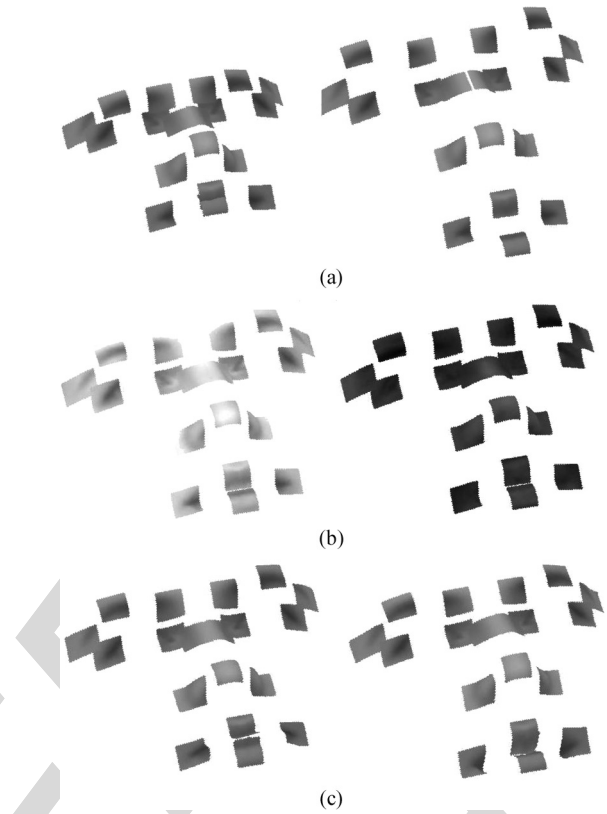


Fig. 3. SFAM learned from the Bosphorus data set. (a) First landmark configuration mode explains variations in terms of the face size and expression. (b) First texture mode explains skin color variations. (c) First range mode explains surface geometry variations, mainly in the nose and mouth regions.

Using the SFAM-1, the fitting algorithm was first applied on
584 the remaining FRGC v1 data sets (i.e., 462 scans from subjects
585 different from those in training). We then tested the algorithm
586 on 1500 facial scans (randomly selected from the FRGC v2 data
587 set) which contain illumination variations and facial expres-
588 sions. Fig. 4 depicts the cumulative distribution of the fitting
589 error for all 15 landmarks. Note that most landmarks were
590 automatically localized within 9 mm in both tests. Table III
591 summarizes the mean, the standard deviation of localization
592 errors associated with each landmark tested on FRGC v1 and
593 FRGC v2, and a comparison with the result achieved by a
594 curvature-analysis-based landmarking method [31]. The first
595 two columns show the mean and the standard deviation of lo-
596 calization error for each landmark (d_i) from our method while
597 the third column depicts the results achieved by the curvature-
598 analysis-based method. Note that the mean localization error
599 of all landmarks is less than 5 mm. An increase in the mean
600 and the standard deviation of errors generated in the experiment
601 on FRGC v2 compared with FRGC v1 was mainly caused by
602 uncontrolled illumination and facial expressions on tested facial
603 scans. Compared to curvature-analysis-based method, which
604 only uses geometry knowledge on faces, the proposed approach
605 can locate a larger number of landmarks. The mean and stan-
606 dard deviation in localization errors from our method were
607 smaller when compared to those obtained from the curvature-
608 analysis-based method except for the nose tip, which is the
609 most shape salient landmark on a face. Fig. 5 illustrates selected
610 landmark localization results from the first two experiments. 611

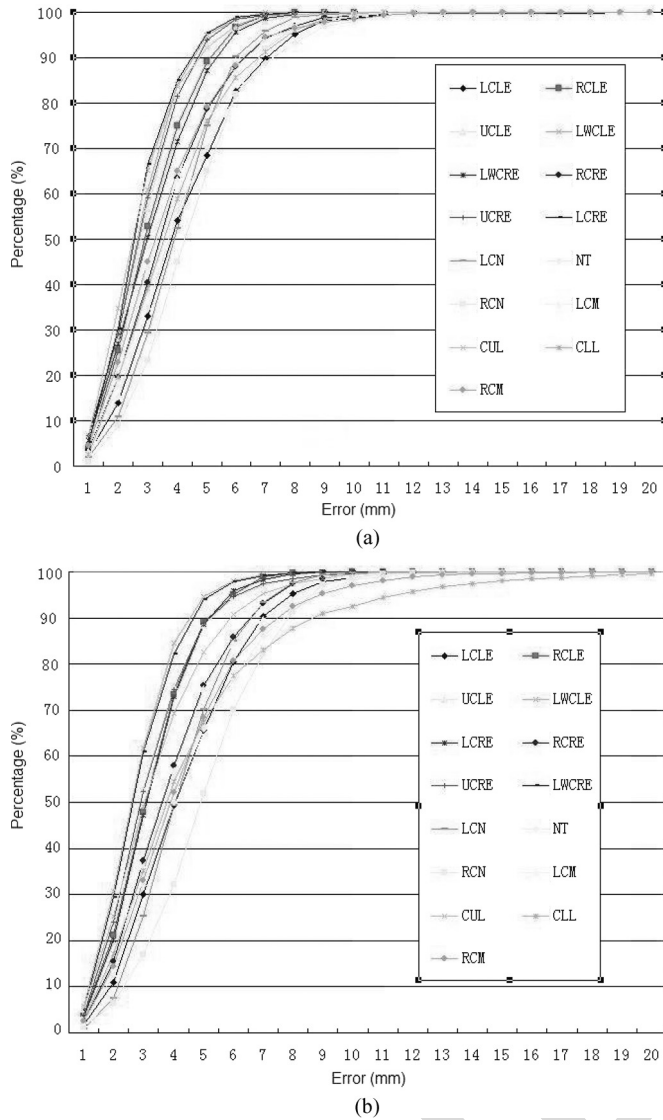


Fig. 4. Cumulative error distribution of the error for the 15 landmarks using (a) FRGC v1 and (b) FRGC v2. The symbols used are the following: LCLE—left corner of left eye, RCLE—right corner of left eye, UCLE—upper corner of left eye, LWCLE—lower corner of left eye, LCRE—left corner of right eye, RCRE—right corner of right eye, UCRE—upper corner of right eye, LWCRC—lower corner of right eye, LCN—left corner of nose, NT—nose tip, RCN—right corner of nose, LCM—left corner of mouth, CUL—center of upper lip, CLL—center of lower lip, and RCM—right corner of mouth.

The third experiment was carried out on the BU-3-DFE data set. Recall that 143 facial scans from the first five male subjects and six female subjects were used for training the SFAM-2. From the remaining 89 subjects, 1157 facial scans in total were used for testing. Each tested subject has a neutral expression and the six universal facial expressions at the intensity levels three and four. Fig. 6 illustrates several localization examples having facial expressions. Fig. 7 depicts the effect of expressions on landmarking accuracy. Note that landmarks with less deformation in expressions were better localized (i.e., eye corner, nose tip, and nose corner). Mouth corners and the middle of the lower lip were detected with the worst accuracy, and the largest standard deviation was observed in scans displaying surprise because of the large mouth displacement and ample deformation in this region. Table IV summarizes

TABLE III
COMPARISON OF MEAN ERROR AND STANDARD DEVIATION ASSOCIATED WITH EACH OF THE 15 LANDMARKS ON THE FRGC DATA SET

ID	Mean (std) mm		
	I	II	III
LCLE	4.17 (2.13)	4.31 (2.05)	7.87 (4.06)
RCLE	3.07 (1.42)	3.21 (1.44)	3.68 (1.98)
UCLE	2.92 (1.39)	3.17 (1.66)	- (-)
LWCLE	2.76 (1.21)	2.75 (1.31)	- (-)
LCRE	3.15 (1.56)	3.24 (1.43)	3.75 (1.96)
RCRE	3.67 (1.90)	3.89 (2.04)	6.59 (3.42)
UCRE	2.84 (1.45)	3.18 (1.63)	- (-)
LWCRC	2.68 (1.21)	2.83 (1.38)	- (-)
LSN	3.96 (1.65)	4.21 (1.71)	6.50 (5.36)
NT	4.11 (2.20)	4.43 (2.56)	1.93 (1.16)
RSN	4.39 (1.85)	5.07 (2.36)	6.81 (5.31)
LCM	3.61 (1.92)	4.09 (2.32)	9.10 (7.58)
CUL	2.74 (1.42)	3.37 (1.89)	- (-)
CLL	3.81 (1.97)	4.65 (3.41)	- (-)
RCM	3.58 (1.99)	4.34 (2.50)	8.83 (7.59)



Fig. 5. Landmark localization examples from the FRGC data set.

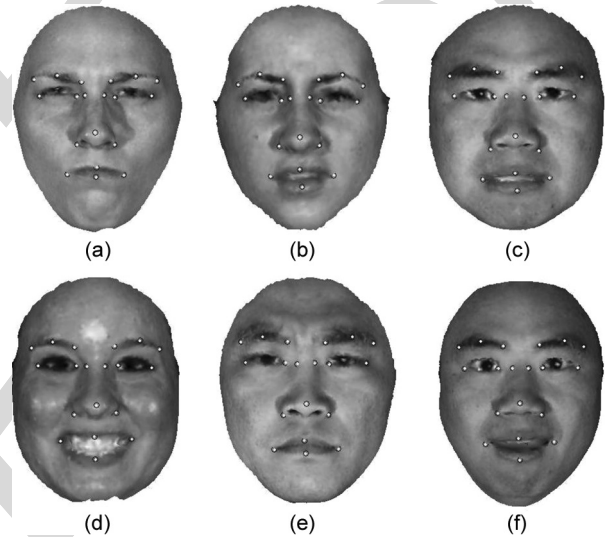


Fig. 6. Landmarking examples from the BU-3-DFE data set with expressions. (a) Anger. (b) Disgust. (c) Fear. (d) Happiness. (e) Sadness. (f) Surprise.

the mean error and the standard deviation of the proposed landmarking algorithm compared to the mean error of a PDM [21], which is trained with 150 face scans and tested on the remainder of the BU-3-DFE data set. Because of the use of local texture and geometry knowledge in our approach, there is a significant decrease in the localization errors. The mean error for all 19 landmarks is within 10 mm while most of standard deviations are lower than 5 mm. The localization accuracy of landmarks in the rigid face region is comparable to those of the corresponding landmarks automatically localized in FRGC.

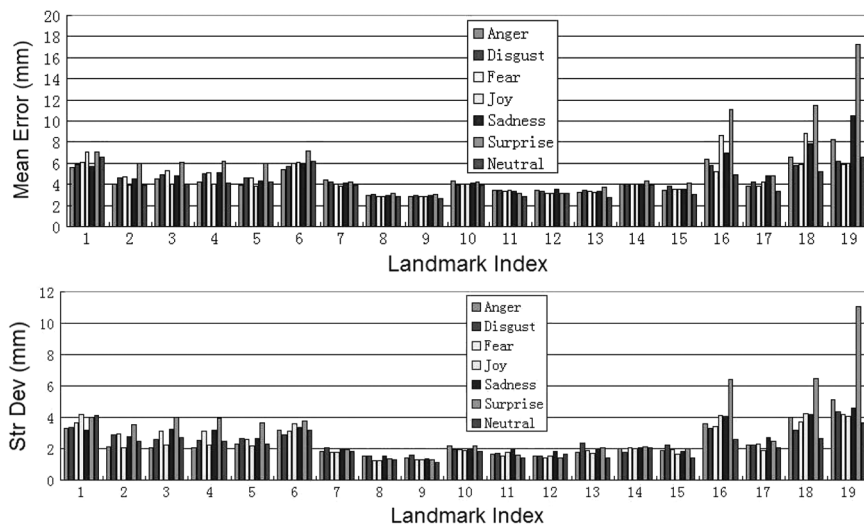


Fig. 7. Landmarking accuracy on different expressions with the BU-3-DFE data set. 1: Left corner of left eyebrow. 2: Middle of left eyebrow. 3: Right corner of left eyebrow. 4: Left corner of right eyebrow. 5: Middle of left eyebrow. 6: Right corner of right eyebrow. 7: Left corner of left eye. 8: Right corner of left eye. 9: Left corner of right eye. 10: Right corner of right eye. 11: Left nose saddle. 12: Right nose saddle. 13: Left corner of nose. 14: Nose tip. 15: Right corner of nose. 16: Left corner of mouth. 17: Middle of upper lip. 18: Right corner of mouth. 19: Middle of lower lip.

TABLE IV
MEAN ERROR AND THE CORRESPONDING STANDARD DEVIATION (IN MILLIMETERS) OF THE 19 AUTOMATICALLY LOCALIZED LANDMARKS ON THE FACIAL SCANS FROM THE BU-3-DFE DATA SET (ALL EXPRESSIONS INCLUDED)

ID	Mean	Std	Mean	ID	Mean	Std	Mean
1	6.26	3.72	-	11	3.30	1.70	-
2	4.58	2.82	-	12	3.27	1.56	-
3	4.87	2.99	-	13	3.32	1.94	-
4	4.88	2.97	-	14	4.04	1.99	8.83
5	4.51	2.77	-	15	3.62	1.91	-
6	6.07	3.35	-	16	7.15	4.64	-
7	4.11	1.89	20.46	17	4.19	2.34	-
8	2.93	1.40	12.11	18	7.52	4.75	-
9	2.90	1.36	11.89	19	8.82	7.12	-
10	4.07	2.00	19.38				

TABLE V
MEAN ERROR AND THE CORRESPONDING STANDARD DEVIATION ASSOCIATED WITH EACH OF THE 19 AUTOMATICALLY LOCALIZED LANDMARKS ON THE FACIAL SCANS FROM THE BOSPHORUS DATA SET UNDER OCCLUSION

ID	Mean (Std) <i>mm</i>		ID	Mean (Std) <i>mm</i>	
	I	II		I	II
1	9.66 (6.08)	11.95 (8.85)	11	7.50 (3.60)	7.56 (3.88)
2	8.29 (3.92)	8.47 (4.39)	12	7.58 (3.63)	6.92 (4.02)
3	7.33 (3.41)	7.15 (3.36)	13	6.35 (3.11)	7.19 (2.99)
4	7.02 (3.23)	6.77 (3.38)	14	8.46 (3.64)	8.39 (3.64)
5	8.21 (4.27)	8.20 (4.45)	15	8.03 (3.31)	7.79 (3.36)
6	9.74 (5.23)	10.05 (6.08)	16	7.96 (4.18)	9.75 (6.28)
7	7.01 (3.77)	8.83 (6.37)	17	8.67 (4.84)	9.01 (4.93)
8	6.25 (3.42)	6.87 (4.21)	18	8.21 (4.25)	9.65 (4.97)
9	6.44 (3.08)	6.51 (3.58)	19	10.41 (5.37)	10.61 (5.61)
10	7.46 (3.56)	7.86 (4.73)			

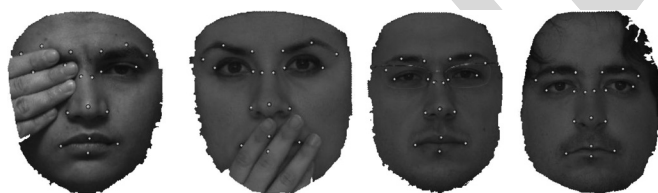


Fig. 8. Landmarking examples from the Bosphorus data set with occlusion. From left to right, faces are occluded in the eye region, in the mouth region, by glasses, and by hair.

637 The last experiment tested the fitting algorithm using the
 638 SFAM-3 to locate 19 landmarks on 3-D scans under occlusion
 639 from the Bosphorus data set. Fig. 8 illustrates several localiza-
 640 tion examples under occlusion. This experiment was carried out
 641 on 292 scans from all the subjects excluding the ones used for
 642 training in the Bosphorus data set. To evaluate the efficiency of
 643 our proposed occlusion classifier, the fitting algorithm was first
 644 tested with occlusion knowledge directly provided by the data
 645 set and, then, with occlusion knowledge from our occlusion
 646 detection and classification algorithm (see Table V). In both
 647 configurations, the mean errors ranged from 6 to 11 mm.
 648 Meanwhile, 71.4% of the landmarks were localized with a 10-

mm precision, and 97% of the landmarks were located with a 49
 20-mm precision. Note that there is only a slight increase on 650
 mean error and standard deviation on average when we switch 651
 the accurate knowledge on occlusion as provided by the data 652
 set to the one provided by the proposed occlusion detection 653
 algorithm described in Section IV. 654

E. Discussion

We studied the influence of landmark configuration on the 656
 landmarking results (see Table VI). Three sets of landmarks, 657
 consisting of 5, 9, and 15 landmarks, respectively, were tested 658
 on 100 facial scans randomly selected from the FRGC v1 data 659
 set. The subjects depicted in these scans were different from 660
 the subjects used for training the SFAM, which is the SFAM-1 661
 described in Section V-C. From Table VI, it is evident that the 662
 mean errors remain stable (with a slight decrease in some cases) 663
 when the number of landmarks increases from 5 to 15. Mean- 664
 while, there exists an upper bound on the number of landmarks, 665
 which depends upon the distinctiveness of landmarks so far 666
 characterized in this paper based on their global configurational 667

TABLE VI
INFLUENCE OF LANDMARK CONFIGURATION
ON MEAN ERRORS (IN MILLIMETERS)

	Mean(Std) <i>mm</i>		
	I	II	III
LCLE	- (-)	4.96 (2.33)	4.79 (2.15)
RCLE	3.20 (1.73)	3.15 (1.70)	3.14 (1.70)
UCLE	- (-)	- (-)	2.74 (1.30)
LWCLE	- (-)	- (-)	2.46 (1.32)
LCRE	3.60 (1.61)	3.56 (1.63)	3.56 (1.61)
RCRE	- (-)	3.73 (1.77)	3.57 (1.55)
UCRE	- (-)	- (-)	2.66 (1.08)
LWCRE	- (-)	- (-)	2.49 (1.15)
LSn	- (-)	3.92 (1.51)	3.91 (1.52)
NT	4.72 (2.58)	4.46 (2.63)	4.67 (2.51)
RSN	- (-)	4.55 (2.01)	4.41 (2.19)
LCM	3.89 (2.57)	4.07 (2.54)	3.89 (2.57)
CUL	- (-)	- (-)	2.70 (1.62)
CLL	- (-)	- (-)	4.10 (2.18)
RCM	3.77 (2.55)	3.71 (2.55)	3.75 (2.56)

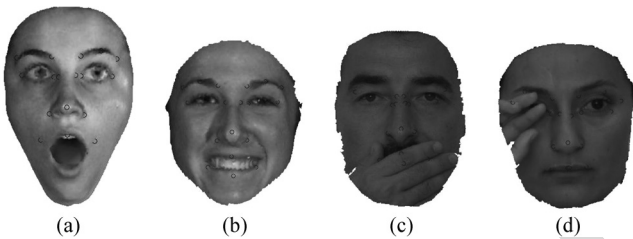


Fig. 9. Selected examples of failure cases. Facial data with (a) surprise, (b) happiness, (c) occlusion in mouth region, and (d) occlusion in eye region.

relationships and their local properties in terms of texture and geometric shape.

The computation time of the proposed algorithm for localizing landmarks on a scan (coded in Matlab) is around 10 min on a desktop PC with Intel Core i7-870 CPU and 8-GB RAM. The time consumed in Step 1 of the fitting algorithm is 130 s on average. It takes 70 to 96 s to compute the correlation meshes in Step 4, depending on the density of the point clouds. The computation time for the optimization of the objective function mainly depends on the speed of convergence. Over 99% of the cases converge within 2000 iterations or 422 s on average.

Fig. 9 illustrates several failure cases of landmarking under different conditions. Cases (a) and (b) are mainly due to ample deformation on the mouth region when faces display exaggerated expressions. The morphology model in the SFAM learns major variation modes from a mixture of expressions and subject identities and does not contain a specific mode for deformation caused by a specific facial expression. When fitting an SFAM on a facial scan having exaggerated facial morphology deformation (e.g., when displaying happiness and surprise), the fitting algorithm sometimes cannot generate morphology instances which approximate these extreme deformations in the mouth region. Cases (c) and (d) are mainly due to information loss in the fitting process when occlusion occurs. The occluded local regions are excluded in the fitting algorithm. Thus, the prediction of morphology parameters uses less information and is not as accurate and robust to local minima as the prediction when there is no occlusion.

We also studied the reproducibility and the corresponding accuracy of manual landmarking. For this purpose, 11 subjects were asked to manually label the 15 landmarks as defined in Fig. 5 on the same 10 facial scans randomly selected from FRGC v1. We then computed the mean error and the corresponding standard deviation of these manually labeled landmarks based on their mean landmark positions. The mean error of these manually labeled 15 landmarks was 2.49 mm with the associated standard deviation at 1.34 mm. In comparison, our localization technique achieved a mean error of 3.43 mm with the corresponding standard deviation of 1.68 mm on the same data set.

Compared to previous 3-D face landmarking algorithms [7], [8], [10], [17], [19], [21], [31], [32], our SFAM-based algorithm is a general data-driven 3-D landmarking framework which encodes the configurational relationships of the landmarks and their local properties in terms of texture and shape by a statistical learning approach instead of using heuristics directly embedded within the algorithm. Thus, our algorithm is more flexible and enables localizing landmarks which are not necessarily shape prominent or texture salient.

VI. CONCLUSION

In this paper, we have presented a general learning-based framework for 3-D face landmarking which proposes to characterize, through a statistical model called SFAM, the configurational relationships between the landmarks as well as their local properties in terms of texture and shape. The fitting algorithm locates the landmarks by maximizing the *a posteriori* probability through the optimization of an objective function. The effectiveness of the framework has been demonstrated in the presence of facial expressions and partial occlusions. Consideration of both the global and local properties helps to characterize landmarks deformed under expressions. Furthermore, partial occlusion can be easily taken into account in the objective function provided that the occlusion probability around each landmark can be estimated. Based on this evidence, we have also introduced a 3-D facial occlusion detection and classification algorithm which exhibited a 93.8% classification accuracy on the Bosphorus data set. This detection is based on local shape similarity between local ranges of an input 3-D facial scan and the instances synthesized from the SFAM. The effectiveness of our technique was supported by the experiments on the FRGC data set (v1 and v2), BU-3-DFE containing expressions, and the Bosphorus data set containing partial occlusion.

In this paper, local range and texture maps were used as simple descriptors of local shape and texture around a landmark. In future work, we plan to further improve landmark localization accuracy in considering other descriptors. We also plan to study the generalization capability of the proposed method.

ACKNOWLEDGMENT

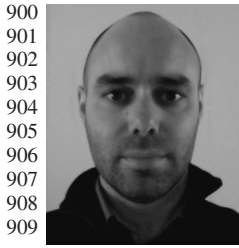
The authors would like to thank the anonymous reviewers for their comments which greatly contributed to the improvement of this paper.

REFERENCES

- 750
- 751 [1] A. A. Salah, H. Cinar, L. Akarun, and B. Sankur, "Robust facial landmarking for registration," *Ann. Telecommun.*, vol. 62, no. 1/2, pp. 1608–1633, 2007.
- 752
- 753
- 754 [2] R. S. Feris, J. Gemmell, K. Toyama, and V. Kruger, "Hierarchical wavelet networks for facial feature localization," in *Proc. 5th IEEE Int. Conf. Autom. Face Gesture Recog.*, Washington, DC, May 20–21, 2002, pp. 125–130.
- 755
- 756
- 757
- 758 [3] F. Y. Shih and C. Chuang, "Automatic extraction of head and face boundaries and facial features," *Inf. Sci.*, vol. 158, pp. 117–130, Jan. 2004.
- 759
- 760 [4] L. Wiskott, J. M. Fellous, N. Kruger, and C. von der Malsburg, "Face recognition by elastic bunch graph matching," *IEEE Trans. Pattern Anal. Mach. Intell.*, vol. 19, no. 7, pp. 775–779, Jul. 1997.
- 761
- 762
- 763 [5] C. Tu and J. J. Lien, "Automatic location of facial feature points and synthesis of facial sketches using direct combined model," *IEEE Trans. Syst., Man, Cybern. B, Cybern.*, vol. 40, no. 4, pp. 1158–1169, Aug. 2010.
- 764
- 765
- 766 [6] K. Bowyer, K. Chang, and P. Flynn, "A survey of approaches and challenges in 3D and multi-modal 3D +2D face recognition," *Comput. Vis. Image Understand.*, vol. 101, no. 1, pp. 1–15, Jan. 2006.
- 767
- 768
- 769 [7] J. D'House, J. Colineau, C. Bichon, and B. Dorizzi, "Precise localization of landmarks on 3D faces using Gabor wavelets," in *Proc. Int. Conf. Biometrics: Theory, Appl., Syst.*, Crystal City, VA, Sep. 27–29, 2007, pp. 1–6.
- 770
- 771
- 772 [8] T. Faltemier, K. Bowyer, and P. Flynn, "Rotated profile signatures for robust 3D feature detection," in *Proc. 8th IEEE Int. Conf. Autom. Face Gesture Recog.*, Amsterdam, The Netherlands, Sep. 17–19, 2008, pp. 1–7.
- 773
- 774
- 775 [9] L. Farkas, *Anthropometry of the Head and Face*, L. G. Farkas, Ed., 2nd ed. New York: Raven, 1994.
- 776
- 777 [10] C. Xu, T. Tan, Y. Wang, and L. Quan, "Combining local features for robust nose location in 3D facial data," *Pattern Recognit. Lett.*, vol. 27, no. 13, pp. 1487–1494, Oct. 2006.
- 778
- 779
- 780 [11] D. Colbry, G. Stockman, and A. Jain, "Detection of anchor points for 3D face verification," in *Proc. IEEE Comput. Soc. Conf. Comput. Vis. Pattern Recog.*, San Diego, CA, Jun. 20–25, 2005, pp. 118–124.
- 781
- 782
- 783 [12] T. F. Cootes, G. Edwards, and C. J. Taylor, "Active appearance models," *IEEE Trans. Pattern Anal. Mach. Intell.*, vol. 23, no. 6, pp. 681–685, Jun. 2001.
- 784
- 785
- 786 [13] T. F. Cootes, C. J. Taylor, D. H. Cooper, and J. Graham, "Active shape models—Their training and application," *Comput. Vis. Image Understand.*, vol. 61, no. 1, pp. 38–59, Jan. 1995.
- 787
- 788
- 789 [14] D. Cristinacce and T. F. Cootes, "Automatic feature localisation with constrained local models," *Pattern Recognit.*, vol. 41, no. 10, pp. 3054–3067, Jan. 2008.
- 790
- 791
- 792 [15] V. Blanz and T. Vetter, "A morphable model for the synthesis of 3D faces," in *Proc. 26th Annu. Conf. Comput. Graph. Interactive Techn.*, Los Angeles, CA, Aug. 8–13, 1999, pp. 187–194.
- 793
- 794
- 795 [16] J. A. Nelder and R. Mead, "A simplex method for function minimization," *Comput. J.*, vol. 7, no. 4, pp. 308–313, Jan. 1965.
- 796
- 797 [17] S. Jahanbin, A. C. Bovik, and H. Choi, "Automated facial feature detection from portrait and range images," in *Proc. IEEE Southwest Symp. Image Anal. Interpretation*, Santa Fe, NM, Mar. 24–26, 2008, pp. 25–28.
- 798
- 799
- 800 [18] Z. Zhang, "Iterative point matching for registration of free-form curves and surfaces," *Int. J. Comput. Vis.*, vol. 13, no. 2, pp. 119–152, Oct. 1994.
- 801
- 802 [19] H. Dibeklioglu, A. A. Salah, and L. Akarun, "3D facial landmarking under expression, pose, and occlusion variations," in *Proc. IEEE Int. Conf. Biometrics: Theory, Appl. Syst.*, Arlington, VA, Sep. 29–Oct. 1, 2008, pp. 1–6.
- 803
- 804
- 805 [20] X. Lu, A. Jain, and D. Colbry, "Matching 2.5D face scans to 3D models," *IEEE Trans. Pattern Anal. Mach. Intell.*, vol. 28, no. 1, pp. 31–43, Jan. 2006.
- 806
- 807
- 808 [21] P. Nair and A. Cavallaro, "3D face detection, landmark localization, and registration using a point distribution model," *IEEE Trans. Multimedia*, vol. 11, no. 4, pp. 611–623, Jun. 2009.
- 809
- 810
- 811 [22] A. Colombo, C. Cusano, and R. Schettini, "3D face detection using curvature analysis," *Pattern Recognit.*, vol. 39, no. 3, pp. 444–455, Mar. 2006.
- 812
- 813 [23] S. Jahanbin, H. Choi, R. Jahanbin, and A. C. Bovik, "Automated facial feature detection and face recognition using Gabor features on range and portrait images," in *Proc. Int. Conf. Image Process.*, San Diego, CA, 2008, pp. 2768–2771.
- 814
- 815
- 816
- 817 [24] V. Bevilacqua, P. Casorio, and G. Mastronardi, "Extending Hough transform to a points cloud for 3D-face nose-tip detection," in *Proc. Int. Conf. Adv. Intell. Comput. Theories Appl.*, Shanghai, China, Sep. 15–18, 2008, pp. 1200–1209.
- 818
- 819
- 820
- 821 [25] Y. Wang, C. Chua, and Y. Ho, "Facial feature detection and face recognition from 2D and 3D images," *Pattern Recognit. Lett.*, vol. 23, no. 10, pp. 1191–1202, Aug. 2002.
- 822
- 823
- 824 [26] B. Gokberk, H. Dutagaci, A. Ulas, L. Akarun, and B. Sankur, "Representation plurality and fusion for 3D face recognition," *IEEE Trans. Syst., Man, Cybern. B, Cybern.*, vol. 38, no. 1, pp. 155–173, Feb. 2008.
- 825
- 826
- 827 [27] C. Boehnen and T. Russ, "A fast multi-modal approach to facial feature detection," in *Proc. IEEE Workshop Appl. Comput. Vis.*, Breckenridge, CO, Jan. 5–7, 2005, pp. 135–142.
- 828
- 829
- 830 [28] I. A. Kakadiaris, G. Passalis, G. Toderici, M. Murtuza, Y. Lu, N. Karampatziakis, and T. Theoharis, "Three-dimensional face recognition in the presence of facial expressions: An annotated deformable model approach," *IEEE Trans. Pattern Anal. Mach. Intell.*, vol. 29, no. 4, pp. 640–649, Apr. 2007.
- 831
- 832
- 833
- 834
- 835 [29] M. L. Koudelka, M. W. Koch, and T. D. Russ, "A prescreener for 3D face recognition using radial symmetry and the Hausdorff fraction," in *Proc. Workshop Comput. Vis. Pattern Recog.*, San Diego, CA, Jun. 20–25, 2005, p. 168.
- 836
- 837
- 838
- 839
- 840 [30] X. Lu and A. K. Jain, "Multimodal facial feature extraction for automatic 3D face recognition," Michigan State Univ., East Lansing, MI, Tech. Rep. MSU-CSE-05-22, 2005.
- 841
- 842
- 843 [31] P. Szeptycki, M. Ardabilian, and L. Chen, "A coarse-to-fine curvature analysis-based rotation invariant 3D face landmarking," in *Proc. 3rd Int. Conf. Biometrics: Theory, Appl. Syst.*, Washington, DC, 2009, pp. 1–6.
- 844
- 845
- 846 [32] X. Lu and A. Jain, "Automatic feature extraction for multiview 3D face recognition," in *Proc. 7th Int. Conf. Autom. Face Gesture Recog.*, Southampton, U.K., Apr. 2–6, 2006, pp. 585–590.
- 847
- 848
- 849
- 850 [33] Y. Sun and L. Yin, "Facial expression recognition based on 3D dynamic range model sequences," in *Proc. 10th Eur. Conf. Comput. Vis.*, Marseille, France, Oct. 12–18, 2008, pp. 58–71.
- 851
- 852
- 853 [34] R. Niese, A. A. Hamadi, F. Aziz, and B. Michaelis, "Robust facial expression recognition based on 3D supported feature extraction and SVM classification," in *Proc. Int. Conf. Autom. Face Gesture Recog.*, Amsterdam, The Netherlands, Sep. 17–19, 2008, pp. 1–7.
- 854
- 855
- 856 [35] P. J. Phillips, P. J. Flynn, T. Scruggs, K. W. Bowyer, J. Chang, K. Hoffman, J. Marques, J. Min, and W. Worek, "Overview of the face recognition grand challenge," in *Proc. IEEE Comput. Soc. Conf. Comput. Vis. Pattern Recog.*, San Diego, CA, Jan. 20–25, 2005, vol. 1, pp. 947–954.
- 857
- 858
- 859 [36] L. Yin, X. Wei, Y. Sun, J. Wang, and M. Rosato, "A 3D facial expression database for facial behavior research," in *Proc. 7th Int. Conf. Autom. Face Gesture Recog.*, Southampton, U.K., Apr. 10–12, 2006, pp. 211–216.
- 860
- 861
- 862 [37] A. Savran, N. Alyuz, H. Dibeklioglu, O. Celiktutan, B. Gokberk, B. Sankur, and L. Akarun, "Bosphorus database for 3D face analysis," in *Proc. 1st COST 2101 Workshop Biometrics Identity Manage.*, 2008, pp. 47–56.
- 863
- 864
- 865
- 866 [38] P. Soille, *Morphological Image Analysis: Principles and Applications*. New York: Springer-Verlag, 1999.
- 867
- 868 [39] S. Z. Li, *Markov Random Field Modelling in Image Analysis*, 3rd ed. New York: Springer-Verlag, 2009.
- 869
- 870 [40] R. Duda, P. Hart, and D. Stork, *Pattern Classification*. Hoboken, NJ: Wiley, 2001.
- 871
- 872 [41] S. Singer and S. Singer, "Efficient implementation of the Nelder–Mead search algorithm," *Appl. Numer. Anal. Comput. Math.*, vol. 1, no. 2, pp. 524–534, Dec. 2004.
- 873
- 874
- 875 [42] P. Perakis, T. Theoharis, G. Passalis, and I. A. Kakadiaris, "Automatic 3D facial region retrieval from multi-pose facial datasets," in *Proc. Eurographics Workshop 3D Object Retrieval*, Munich, Germany, Mar. 30–Apr. 3, 2009, pp. 37–44.
- 876
- 877
- 878
- 879 [43] P. Perakis, G. Passalis, T. Theoharis, G. Toderici, and I. A. Kakadiaris, "Partial matching of interpose 3D facial data for face recognition," in *Proc. 3rd IEEE Int. Conf. Biometrics: Theory, Appl. Syst.*, Arlington, VA, Sep. 28–30, 2009, pp. 1–8.
- 880
- 881
- 882
- 883 [44] P. Sinha, B. Balas, Y. Ostrovsky, and R. Russel, "Face recognition by humans: Nineteen results all computer vision researchers should know about," *Proc. IEEE*, vol. 94, no. 11, pp. 1948–1962, Nov. 2006.
- 884
- 885
- 886 [45] M. Turk and A. Pentland, "Eigenfaces for recognition," *J. Cogn. Neurosci.*, vol. 3, no. 1, pp. 71–86, Jan. 1991.
- 887



Xi Zhao (S'XX) received the B.Sc. and M.Sc. degrees (with honors) from the School of Electronic and Information Engineering, Xi'an Jiaotong University, Xi'an, China, in 2003 and 2007, respectively, and the Ph.D. degree (with honors) in computer science from Ecole Centrale Lyon, Ecully, France, in 2010. He is currently conducting research as a Postdoctoral Fellow at the Computational Biomedicine Laboratory, University of Houston, Houston, TX. His research interests include 3-D face analysis, statistical pattern analysis, and computer vision.



Emmanuel Dellandréa received the Master and Engineer degrees in computer science and the Ph.D. degree in computer science from Université de Tours, Tours, France, in 2000 and 2003, respectively.

In 2004, he joined Ecole Centrale Lyon, Ecully, France, as an Associate Professor. His research interests include multimedia analysis, affective computing, and particularly affect recognition both in image and audio signals as well as facial expression analysis.



Ioannis A. Kakadiaris (SM'XX) received the B.Sc. degree in physics from the University of Athens, Athens, Greece, the M.Sc. degree in computer science from Northeastern University, Boston, MA, and the Ph.D. degree from the University of Pennsylvania, Philadelphia.

He is a Hugh Roy and Lillie Cranz Cullen Professor of Computer Science, Electrical and Computer Engineering, and Biomedical Engineering at the University of Houston (UH), Houston, TX. He joined UH in August 1997 after a postdoctoral fellowship at the University of Pennsylvania. He is the founder of the Computational Biomedicine Laboratory (www.cbl.uh.edu) and, in 2008, directed the Methodist-University of Houston-Weill Cornell Medical College Institute for Biomedical Imaging Sciences (IBIS) (ibis.uh.edu). His research interests include biometrics, nonverbal human behavior understanding, computational life sciences, energy informatics, computer vision, and pattern recognition.

Dr. Kakadiaris is the recipient of a number of awards, including the National Science Foundation Early Career Development Award, Schlumberger Technical Foundation Award, UH Computer Science Research Excellence Award, UH Enron Teaching Excellence Award, and the James Muller Vulnerable Plaque Young Investigator Prize.



Liming Chen (M'XX) was awarded the joint B.Sc. degree in mathematics and computer science from the University of Nantes, Nantes, France, in 1984. He obtained the M.S. and Ph.D. degrees in computer science from the University of Paris 6, Paris, France, in 1986 and 1989, respectively.

He first served as an Associate Professor at the Université de Technologie de Compiègne, Compiègne, France, and then joined Ecole Centrale de Lyon, Ecully, France, as Professor in 1998, where he leads an advanced research team on multimedia computing and pattern recognition. From 2001 to 2003, he also served as Chief Scientific Officer in a Paris-based company, Avivias, specialized in media asset management. In 2005, he served as Scientific expert multimedia in France Telecom R&D China. He has been the Head of the Department of Mathematics and Computer Science since 2007. He has taken out three patents, authored more than 100 publications, and acted as Chairman, PC member, and reviewer in a number of high profile journals and conferences since 1995. He has been a (co)-principal investigator on a number of research grants from the European Union FP programme, French research funding bodies, and local government departments. He has directed more than 15 Ph.D. theses. His current research spans from 2-D/3-D face analysis and recognition and image and video analysis and categorization to affect analysis both in image audio and video.

IEEE
PROOF

AUTHOR QUERIES

AUTHOR PLEASE ANSWER ALL QUERIES

Note that your paper will incur overlength page charges of \$175 per page. The page limit for regular papers is 12 pages, and the page limit for correspondence papers is 6 pages.

- AQ1 = The sentence was rephrased for clarity. Please check if the original thought was retained, and correct if necessary.
- AQ2 = “ANR” is defined as “French National Research Agency.” Please check if appropriate, and correct if necessary.
- AQ3 = “ANR-07-MDCO-009-02” and “ANR-07-SESU-004-03” were captured as grants. Please check if appropriate, and correct if necessary.
- AQ4 = “CNRS” was expanded as “Centre National de la Recherche Scientifique.” Please check if appropriate, and correct if necessary.
- AQ5 = “LIRIS” was expanded as “Laboratoire d’InfoRmatique en Image et Systèmes d’information.” Please check if appropriate, and correct if necessary.
- AQ6 = “UMR” was expanded as “Unité Mixte de Recherche.” Please check if appropriate, and correct if necessary.
- AQ7 = “Boehnen *et al.*” was changed to “Boehnen and Russ.” Please check if appropriate, and correct if necessary.
- AQ8 = “Lu *et al.*” was changed to “Lu and Jain.” Please check if appropriate, and correct if necessary.
- AQ9 = “Nair *et al.*” was changed to “Nair and Cavallaro.” Please check if appropriate, and correct if necessary.
- AQ10 = “MAP” is defined as “maximum a posteriori.” Please check if appropriate, and correct if necessary.
- AQ11 = This sentence was rephrased. Please check if the original thought was retained, and correct if necessary.
- AQ12 = All occurrences of “posteriori probability” were changed to “a posteriori probability.” Please check if appropriate, and correct if necessary.
- AQ13 = All occurrences of “kNN” and “K-NN” were captured as “k-NN” to refer to “k-nearest neighbor” and for consistency. Please check if appropriate, and correct if necessary.
- AQ14 = This sentence was rephrased for clarity. Please check if the original thought was retained, and correct if necessary.
- AQ15 = The caption was restructured for clarity of presentation. Please check if appropriate, and correct if necessary.
- AQ16 = The sentence was rephrased for clarity. Please check if the original thought was retained, and correct if necessary.
- AQ17 = Please provide the IEEE membership history of author Xi Zhao.
- AQ18 = The sentence was rephrased. Please check if the original thought was retained, and correct if necessary.
- AQ19 = Please provide the IEEE membership history of author Liming Chen.
- AQ20 = “Master” was changed to “M.S.” Please check if appropriate, and correct if necessary.
- AQ21 = Please validate the address provided for the Université de Technologie de Compiègne.
- AQ22 = Please validate the address provided for Ecole Centrale de Lyon.
- AQ23 = “EU” was expanded as “European Union.” Please check if appropriate, and correct if necessary.
- AQ24 = Please provide the expanded form of “FP.”
- AQ25 = Please provide the IEEE membership history of author Ioannis A. Kakadiaris.
- AQ26 = “NSF” was expanded as “National Science Foundation.” Please check if appropriate, and correct if necessary.

END OF ALL QUERIES